Alma Mater Studiorum – Università di Bologna

Dipartimento di Ingegneria dell'Energia Elettrica e dell'Informazione

Dottorato di Ricerca in Ingegneria Elettrotecnica

Ciclo XXVI

Settore Concorsuale di afferenza: 09/E1

Settore Scientifico disciplinare: ING-IND/31

ARBITRARY WAVEFORM MULTILEVEL GENERATOR FOR HIGH VOLTAGE HIGH FREQUENCY PLASMA ACTUATORS

di

Filopimin Andreas Dragonas

Tutor: Gabriele Grandi Coordinatore: Domenico Casadei

Co-Tutor: Gabriele Neretti

Anno Esame Finale 2014

Preface

This dissertation presents the theory and the conducted activity that lead to the construction of a high voltage high frequency arbitrary waveform voltage generator. The generator has been specifically designed to supply power to a wide range of plasma actuators. The system has been completely designed, manufactured and tested at the Department of Electrical, Electronic and Information Engineering of the University of Bologna.

The generator structure is based on the single phase cascaded H-bridge multilevel topology and is comprised of 24 elementary units that are series connected in order to form the typical staircase output voltage waveform of a multilevel converter. The total number of voltage levels that can be produced by the generator is 49. Each level is 600 V making the output peak-to-peak voltage equal to 28.8 kV. The large number of levels provides high resolution with respect to the output voltage having thus the possibility to generate arbitrary waveforms. Maximum frequency of operation is 20 kHz.

A study of the relevant literature shows that this is the first time that a cascaded multilevel converter of such dimensions has been constructed. Isolation and control challenges had to be solved for the realization of the system.

The biggest problem of the current technology in power supplies for plasma actuators is load matching. Resonant converters are the most used power supplies and are seriously affected by this problem. The manufactured generator completely solves this issue providing consistent voltage output

independently of the connected load. This fact is very important when executing tests and during the comparison of the results because all measures should be comparable and not dependent on matching issues.

The use of the multilevel converter for power supplying a plasma actuator is a real technological breakthrough that has provided and will continue to provide very significant experimental results.

The importance of the generator has been noticed by the aerospace company Alenia Aermacchi (AAM) that has shown interest in the project. During the last year collaboration between our department and AAM was started. Lab tests were conducted in partnership with AAM technicians both at the university as well as at the AAM headquarters. The experimental results showed the great potential of the implemented technology.

Finally, it is a pleasure to mention that AAM was highly convinced by this potential and funded a project for the construction of new generator that is based on the work presented in this dissertation.

Acknowledgements

I would like to express my sincere gratitude to my tutor, Gabriele Grandi for the technical support he has provided through these years.

I'm also thankful to the Lisp lab team headed by professor Carlo Angelo Borghi. A particular thank you to Gabriele Neretti.

Finally, I thank my fantastic parents for supporting me all these years and my beautiful baby for putting up with me through the difficult times and bringing joy to my life every day. Love you.

Table of Contents

List of Figures

Chapter 1

INTRODUCTION

1.1 Plasma

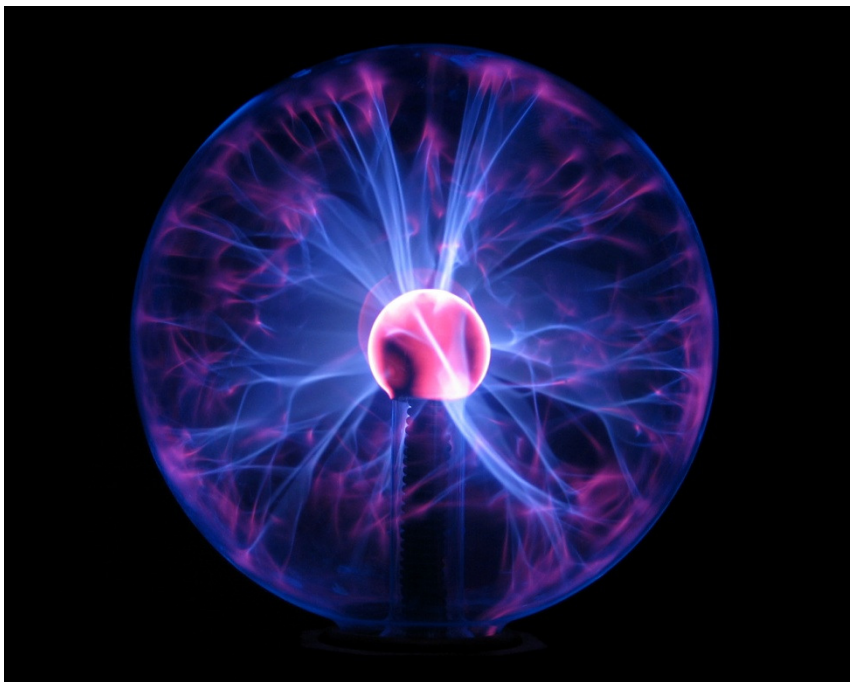

Figure 1.1 A plasma lamp

Plasma (Fig. 1.1) in physics is often defined as the fourth fundamental state of matter with regard to the other three being solid, liquid and gas. A solid substance at constant pressure is generally transformed into liquid by increasing its temperature. Following the same principle by further increasing the temperature a liquid becomes a gas. At a sufficiently high temperature the molecules of the gas decompose forming a cloud of atoms that move independently in casual directions. By increasing the temperature even more the atoms break down

into freely moving charged particles, which are electrons and positive ions. When this event triggers the substance is said to have entered the plasma state.

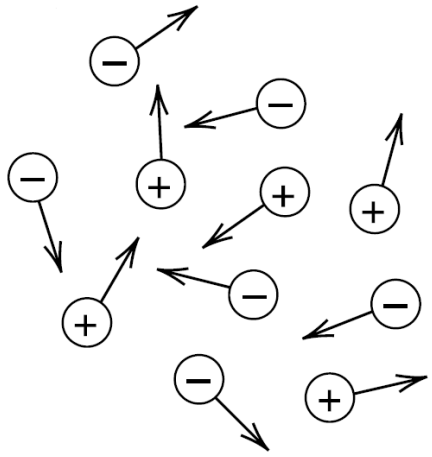

Figure 1.2 Electrons and positive Ions

Although it is the least familiar state of matter for us, inhabitants of planet Earth, plasma is actually the most common state of matter throughout the whole visible universe. Based on the thermodynamic equilibrium state of which the plasma is in, it is divided into two principal categories:

- Thermal plasma, where the heavy charge species like ions often have the same temperature as the electrons;
- Non-thermal plasma, where the electrons' temperature is much higher than that of the heavy charge species.

Thermal plasmas can be for example arcs or radio frequency inductively coupled plasma discharges. They are associated with Joule heating and thermal ionization, and usually occur at high pressure. The temperature can reach around 4,000K to 30,000K. The applications of thermal plasmas

include metal cutting and welding, metal spraying and waste incineration.

When non-thermal plasmas are being produced, the majority of the electrical energy mainly goes into the generations of energetic electrons while the rest of the gas remains at low temperature. Thus, the electron temperature reaches around 105 K. In the meantime ions and neutral species are at room temperature. Thus, non-thermal plasmas can be generated at low pressure and low temperature circumstances. Non-thermal plasma is the subject of this dissertation.

1.2 Dielectric Barrier Discharge

The dielectric barrier discharge [DBD] is a suitable way to generate a stable, confined and homogeneous plasma at high as well as at atmospheric pressure. This method was first introduced in 1857 by Ernst Werner von Siemens for generating ozone.

In order to achieve a DBD appropriate AC voltage has to be applied between two electrodes that are first separated by an insulating material. Fig. 1.3 depicts a schematic DBD setup. Typical voltage levels for these devices are in orders of kV and are usually applied to only one of the two electrodes. The other is anchored to the ground potential. The dielectric material plays a significant role in the formation of the plasma and its quality. Typical materials for this use are polymers such as Kapton and Teflon or even Plexiglas.

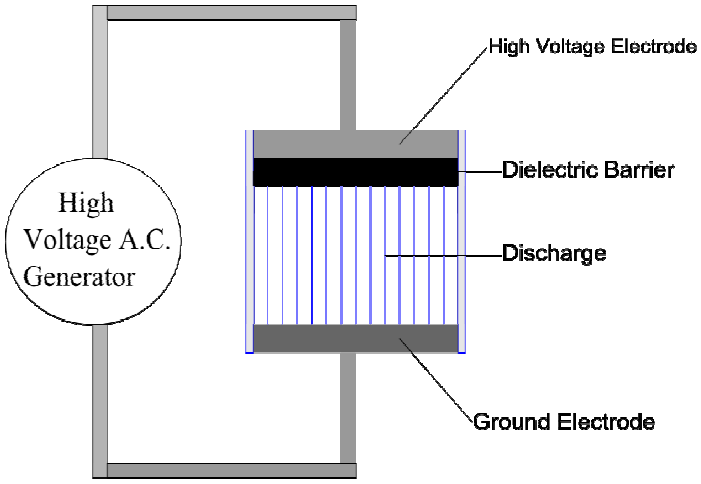

Figure 1.3 The DBD configuration

As depicted in the figure plasma is established directly in the shape of streamer channels, i.e. arcs, and no sparks are formed. This phenomenon is very characteristic and is due to the accumulation of charged species on the dielectric layer that limit the electric field in the gas gap and so the lifespan of the microdischarges cannot exceed few hundreds of nanoseconds.

The use of DC voltages is obviously excluded by the existence of a separating dielectric layer and DBD is usually operated at high frequencies that range from few kHz to even thousands of kHz. The non-thermal plasma produced by a DBD is currently being experimented in different research fields and industrial processes. The relative low temperature of heavy particles that coexist with high energetic electrons and reactive radicals, make this type of plasma very attractive for engineering purposes. Typical plasma uses are:

- plasma etching in microelectronics;
- surface treatment to increase dyeability, wettability and adhesion;

- sterilization of surfaces and gases from bacteria, parasites and molds;
- abatement of pollutants and volatile organic compounds present in combustion processes and cooking activities;
- ozone production;
- food treatment by using pulsed electric fields (PEF) and non-thermal pasteurization;
- plasma biology and plasma medicine for skin, teeth and wounds treatment;
- electro-fluid-dynamic actuators for active flow control.

1.3 Active Flow Control

Active flow control is defined as a way of varying the direction of a flow in order to obtain a desired change. Active flow control is usually applied to affect three types of situation:

- the laminar-to-turbulent transition,
- the separation,
- and the turbulence;

If the laminar to turbulent transition is delayed the effect can be that of reduced drag, which for an aircraft can mean the reduction of the fuel consumption which would lead to longer range and higher travel speed. The main limitation for the maximum achievable lift of a curved airfoil is the separation. The ability of the flow to travel along the shape of the airfoil determines the moment when the separation occurs. Finally the decrease in turbulence can significantly reduce the aerodynamic noise.

When a fluid flows along a solid surface of an object, most of the times the system is studied by separating it into two distinctive parts: a free stream flow at a certain distance from the surface and a boundary layer close to the surface. Usually, the prime boundary layer will be laminar with smooth streamlines. As the fluid moves further downstream the Reynolds number which is a function of the development length increases and at some point transition from laminar to turbulent happens. The point where the transition occurs depends on many factors which include the shape of the surface, the level of turbulence in the free stream flow, and the pressure gradient along the surface. One important way of characterizing this external flow is the dimensionless Reynolds number:

$$Re = \frac{\rho v L}{\mu}$$

Where ρ is fluid density, v is flow velocity, μ is the dynamic viscosity of the fluid and L is the characteristic length of the object.

In function of the shape of the surface, there might be a positive or negative pressure gradient in the boundary layer on the surface. The positive gradient is known as an adverse pressure gradient and leads the flow to separate from the surface. As shown in Fig. 1.4 flow separation happens when the speed in the boundary layer is highly reduced or even zeroed, which significantly increases the drag on the surface.

Flow separation can happen both in laminar as well as in turbulent boundary layers. Turbulent boundary layer has

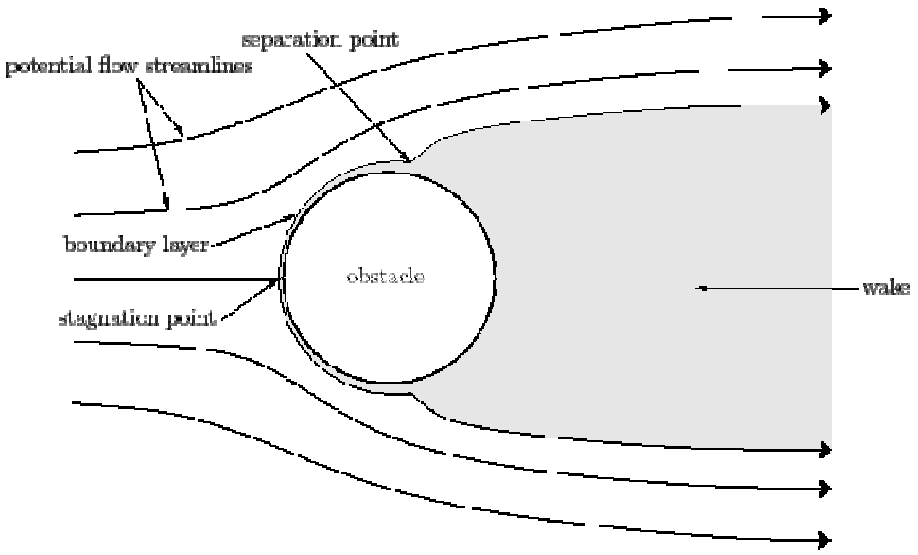

Figure 1.4 Flow Separation

more momentum near the surface than the laminar boundary layer, this makes it more difficult to slow the boundary flow down to the separation speed (close to zero). In the low pressure turbine stage of a jet engine, the flow is fully attached to the airfoils during takeoff and landing. However, at cruising altitudes the Reynolds number decreases to the order of 105 because of the reduced gas density. Part of the flow than becomes laminar can separate early on the blades, and it then can reattach or be separated over the rest of the surface. This phenomenon is usually called the “separation bubble”. Separation makes the turbine highly inefficient. However, if the laminar-to-turbulent transition happens before the separation point, the bubble can be majorly limited. For long distance travels, the high loss of efficiency by separation will can become an important factor on fuel efficiency. Thus flow separation must be limited in order to obtain more economic and environmental acute flights.

Separation can also produce flow instabilities behind bodies of an airfoil or turbine blades. These instabilities generate high amounts of noise. Active flow control to limit the noise

production has been proved effective on a landing-gear strut and in the jet engine exhaust.

1.3.1 The Stall

A stall is a condition in aerodynamics and aviation wherein the angle of attack increases beyond a certain point such that the lift begins to decrease. The angle at which this occurs is called the critical angle of attack. This critical angle is mainly dependent upon the profile of the wing, its shape and its aspect ratio and is typically in the range of 8 to 20 degrees relative to the incoming wind. The critical angle of attack is the angle of attack on the lift coefficient versus angle-of-attack curve at which the maximum lift coefficient occurs. The stall is an extreme case of separation.

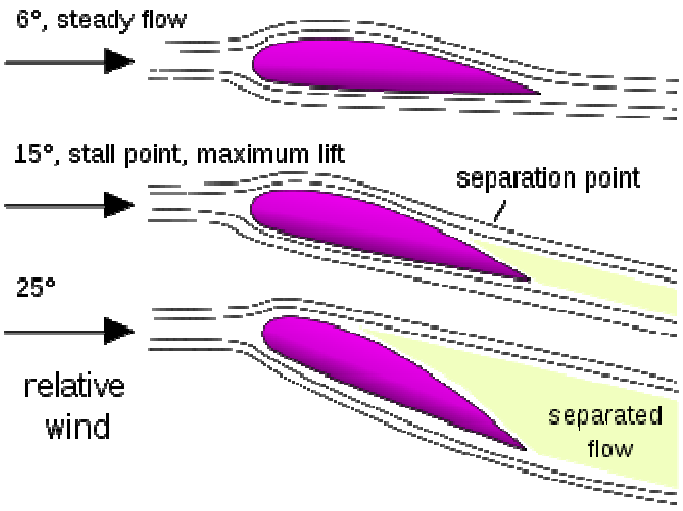

Figure 1.5 The stall phenomenon

Flow separation begins to occur at small angles of attack while attached flow over the wing is still dominant. As angle of attack increases, the separated regions on the top of the wing increase in size and hinder the wing's ability to create

lift. At the critical angle of attack, separated flow is so dominant that further increases in angle of attack produce less lift and vastly more drag. The effect of this phenomenon is reduced or even total uncontrollability of the aircraft that can lead to very dangerous situations. A stall can happen at both low speed and high speed. In particular a critical situation for commercial aircrafts usually happens during landing though high maneuverability aircrafts can also suffer from a stall due to rapid changes in direction during flight. Except for flight training, airplane testing, and aerobatics, a stall is usually an undesirable event. The most common way to prevent it is by deploying spoilers on the aircraft wings (Fig. 1.6).

Figure 1.6 Spoilers on a wing

Spoilers can be of various kinds and shapes and can be positioned in different positions on the wing. A thorough investigation of these systems goes beyond the scope of this dissertation. An important aspect that needs to be highlighted though is that spoilers are composed of moving parts, mainly mechanical and hydraulic components.

The nature of these components makes them susceptible to some common drawbacks. First of all moving parts that are also usually subject to high forces generate friction that can lead to wear or even worse to breakage. Secondly the design of aircrafts is very sensitive to the weight factor which is obviously kept as low as possible while spoilers are heavy objects. Finally the cost of spoilers can be very high.

1.3.2 Plasma Actuators

As presented in the previous section in order to control the air flow on an aircraft wing it is necessary to install spoilers that have certain drawbacks. A new technology that is still under development aims to exceed the limitations posed by mechanical systems and open new paths in the field of fluid dynamics. This technology is a plasma actuator.

Plasma actuators that are used for flow control can be of two types: 1) corona discharge plasma actuator, 2) Dielectric Barrier Discharge plasma actuator. Surface corona discharge actuators have been able to produce electric winds of up to 10m/s and have been studied in literature since the 80s. The main advantage of these devices is their simplicity and that they only need high voltage DC power. The induced wind speed per unit of input power defined as the electro-mechanical efficiency is higher for the corona with respect to a DBD plasma actuator though the maximum velocity of the generated flow is limited by the glow-to-arc transition when the potential difference between the two electrodes is over the threshold.

On the other hand with AC or pulsed voltage supply DBD devices can be very interesting in the active flow control

field because the glow to-arc transition is naturally prevented by the barrier that stops the displacement current.

A non thermal plasma actuator implemented with the use of a DBD is depicted in Fig. 1.7. Like a typical DBD configuration the actuator makes use of two electrodes. One is supplied from a high voltage ac power supply while the other one, the low voltage electrode, is anchored to the ground potential.

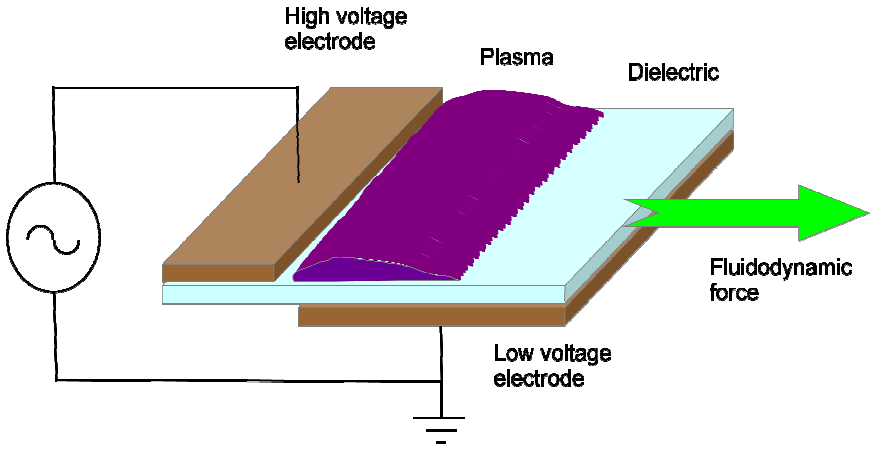

Figure 1.7 A plasma actuator

Furthermore the even though the two electrodes are parallel their position is shifted with respect to the longitudinal axis. In between the two electrodes lies a layer of dielectric material. This material is usually a polymer.

When an alternating high voltage is applied to this setup plasma forms on the surface of the dielectric and stretches longitudinally from the interior edge of the HV electrode. The quality of the plasma depends on the thickness of the dielectric and on the intensity of the applied electric field. As previously explained when plasma forms ions are created. With this particular configuration of the electrodes the ions receive a longitudinal push which gives place to the so called “ionic wind”.

Finally the “ionic wind” generates a fluid dynamic force with direction parallel to the green arrow (Fig. 1.7).

In fluid dynamics and more specifically in air dynamics this effect can be exploited in order to control air flow. A plasma actuator can be placed on a wing taking the place of a spoiler in order to direct the air flow as needed. Flow separation can be controlled in same way as with spoilers and stall situations could be prevented.

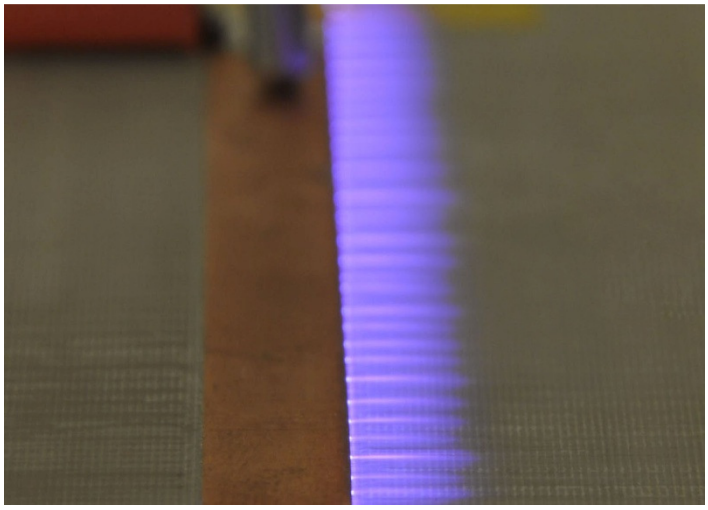

Figure 1.8 Formation of plasma

A plasma actuator used for fluid dynamic purposes exceeds a spoiler in all its drawbacks. It is a purely electrical system with no moving parts thus requiring low maintenance. The weight of the actuator per se is insignificant with respect to the weight of an aircraft’s wing. The heaviest part of such system is the power supply which can be placed though in the fuselage significantly lightening the weight of the wing. Finally, the cost of an actuator which is made of strips of copper and plastic materials is obviously lower than that of a spoiler.

1.4 Power Supplies

In the previous section a small introduction to the dielectric barrier discharge phenomenon was presented as well as the plasma actuator. It was stated and shown that these devices need high voltage and alternating power supplies in order to function. Voltages for these applications usually range between 1 – 50 kV while frequencies start from few kHz to hundreds of kHz. On the other hand currents are low, a few amperes, and they are of impulsive nature. A continuous current is never manifested in such highly capacitive systems.

Typical power supplies for DBDs are power amplifiers that use high voltage transformers or resonant switching converters. Both of these types of power supplies have important drawbacks. First of all, these systems are usually bulky devices built for high power applications that are inefficient when coupled with capacitive loads. In particular, resonant converters have to be fine tuned in order to optimize their performance. The optimum operating point is unique and can significantly change as a result of small load and connection variations. Furthermore, conventional power supplies can only generate a restricted number of voltage waveform types, essentially sinusoidal.

However, the effect of the waveform shape in DBD fluid dynamics actuators is currently being studied. Hence there is strong interest on trying new voltage waveforms which could enhance the induced thrust.

1.5 Multilevel Converters

Multilevel converters are circuits composed of an array of power semiconductors and voltage sources that generate an output voltage with stepped waveforms.

A very important advantage of these converters is the fact that they can reach high output voltage levels while the power semiconductors and the rest of the components must be able to withstand only a fraction of the output voltage. In Fig. 1.9 a 9 level inverter output waveform is shown as well as the each step voltage that forms it.

Multilevel converters can be sorted into three main categories:

- Diode Clamped
- Capacitor Clamped
- Cascaded H-Bridge

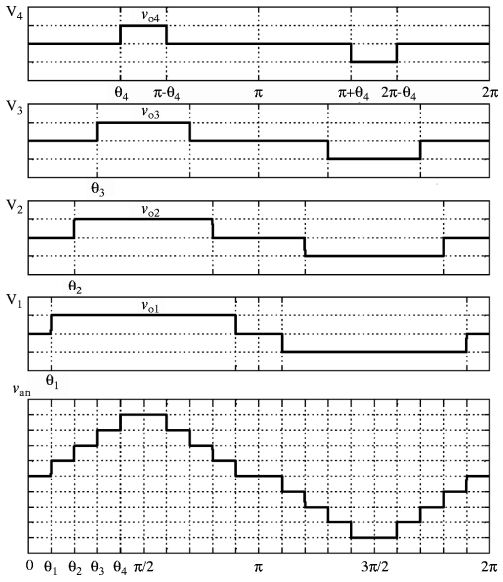

Figure 1.9 Typical multilevel staircase

1.5.1 Diode Clamped

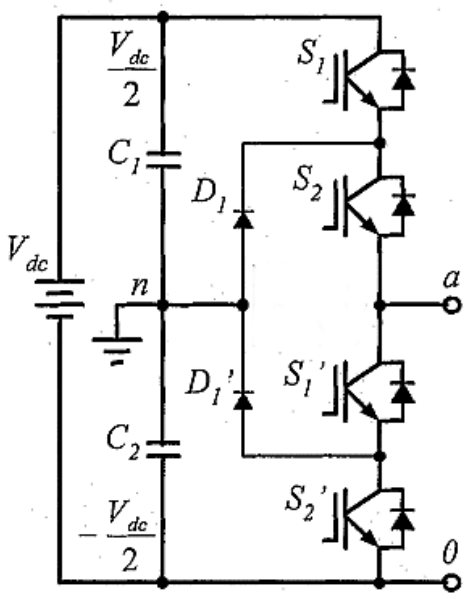

Figure 1.10 Diode clamped topology

Fig. 1.10 shows a three-level diode-clamped inverter. The DC-bus voltage is divided into three levels. Two series-connected bulk capacitors are used for this reason. The middle point *n* can be defined as the neutral point. The output voltage v_{an} has three states: $V_{dc}/2$, 0, and $-V_{dc}/2$. For voltage level $V_{dc}/2$, switches S_1 and S_2 need to be turned on; for $-V_{dc}/2$, switches S_1' and S_2' need to be turned on; and for the 0 level, S_2 and S_1' need to be turned on.

The important components in this circuit are the two diodes D_1 and D_1'. These two diodes clamp the switch voltage to half the level of the dc-bus voltage. When both S_1 and S_2 turn ON, the voltage across *a* and 0 is V_{dc}. In this case, D_1 balances the voltage sharing between S_1' and S_2' with S_1' blocking the

voltage across C_1 and S_2' blocking the voltage across C_2 . Notice that output voltage v_{an} is AC, and v_{an0} is DC (both S_1 and S_2 ON). The difference between v_{an} and v_{an0} is the voltage across C_2, which is $V_{dc}/2$. If the output is removed out between *a* and 0, then the circuit becomes a dc/dc converter, which has three output voltage levels: V_{dc}, $V_{dc}/2$, and 0.

Although each active switching device is only required to block a voltage level of $V_{dc}/(m-1)$, where m is the number of levels, the clamping diodes must have different voltage ratings for reverse voltage blocking. Assuming that each blocking diode voltage rating is the same as the active device voltage rating, the number of diodes required for each phase will be $(m-1) \times (m-2)$. This number represents a quadratic increase in m. When m is sufficiently high, the number of diodes required will make the system impractical to implement.

1.5.2 Capacitor Clamped

Fig. 1.11 illustrates the fundamental building block of a phase-leg capacitor-clamped inverter. The circuit is also called flying capacitor inverter with independent capacitors clamping the device voltage to one capacitor voltage level. This inverter provides a three-level output across *a* and *n*, $V_{dc}/2$, , 0, or $-V_{dc}/2$. For the first one, switches S_1 and S_2 need to be turned on; for $-V_{dc}/2$, switches S_1' and S_2' need to be turned on; and

for the 0 level, either pair (S_1, S_1') or (S_2, S_2') needs to be turned on. Clamping capacitor C_1 is charged when S_1 and S_1' are turned on, and is discharged when S_2 and S_2' are turned on.

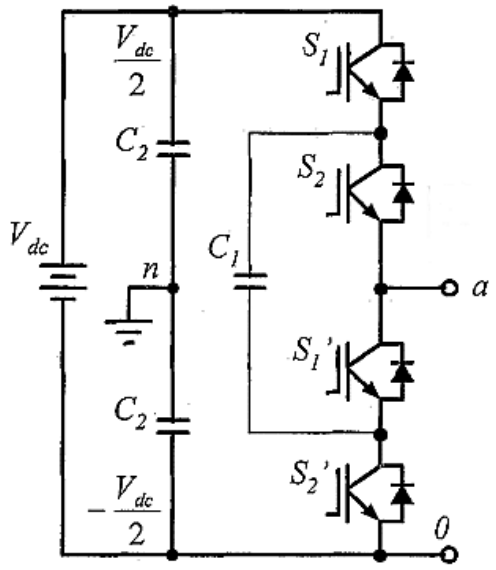

Figure 1.11 Capacitor clamped topology

Similar to diode clamping, the capacitor clamping requires a large number of bulk capacitors to clamp the voltage. Provided that the voltage rating of each capacitor used is the same as that of the main power switch, an m-level converter will require a total of $(m-1) \times (m-2)/2$ clamping capacitors per phase leg in addition to $(m-1)$ main dc-bus capacitors.

1.5.3 Cascaded Multilevel

A different converter topologyh is based on the series connection of single-phase inverters with separate dc sources Fig. 1.12 shows the power circuit for one phase leg of a nine-level inverter with four cells in each phase. The resulting phase voltage is synthesized by the addition of the voltages generated

by the different cells. Each single-phase full-bridge inverter generates three voltages at the output $+V_{dc}$, 0, and $-V_{dc}$. This is made possible by connecting the capacitors sequentially to the ac side via the four power switches. The resulting output ac voltage swings from $-4V_{dc}$ to $+4V_{dc}$ with nine levels, and the staircase waveform is nearly sinusoidal, even without filtering.

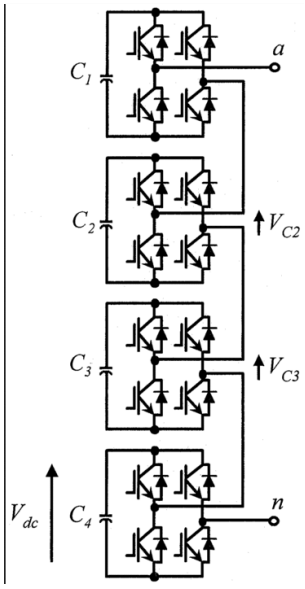

Figure 1.12 Cascaded H-bridge topology

The main advantages of CHB to other topologies are simple control system and the modular structure so that make it first choice for high voltage applications. Also, there is no need for capacitors or diodes to clamp the voltage.

Chapter 2

SYSTEM IMPLEMENTATION: HARDWARE

2.1 Project Design

The multilevel H-bridge converter has been developed and tested in collaboration with the LIMP laboratory. The main technical requirement was to have an AC output voltage in the range of 15 kV with no necessity for load matching. Another requirement to fulfil was to be able to generate arbitrary waveforms. As previously stated testing different kinds of wave shapes is very important in the field of fluid dynamics. Previously used resonant inverter could only generate sinusoidal voltage thus it was impossible to experiment any other waveforms.

In order to meet the given requirements a 49-level cascaded H-bridge inverter was designed. It is composed of 24 elementary units which are series connected on the output in order to generate the multilevel waveform. Each unit can output ±600V. Therefore, when all units are active the output voltage can reach 14,4 kV which means 28,8 kV peak to peak.

The elementary units are composed of three functional parts:

- a power supply stage formed by a 12 V battery pack,
- a regulated voltage step up stage comprised of a flyback converter
- a DC/AC stage which uses an integrated power module.

All the parts that form the elementary unit are implemented with common, low voltage components, which as already noted is a significant advantage of the cascaded H-bridge multilevel topology. Fig. 2.1 depicts the schematic view of the previously described system.

The two waveforms that are shown are intended to visualize the arbitrary output waveforms that the system is designed to generate.

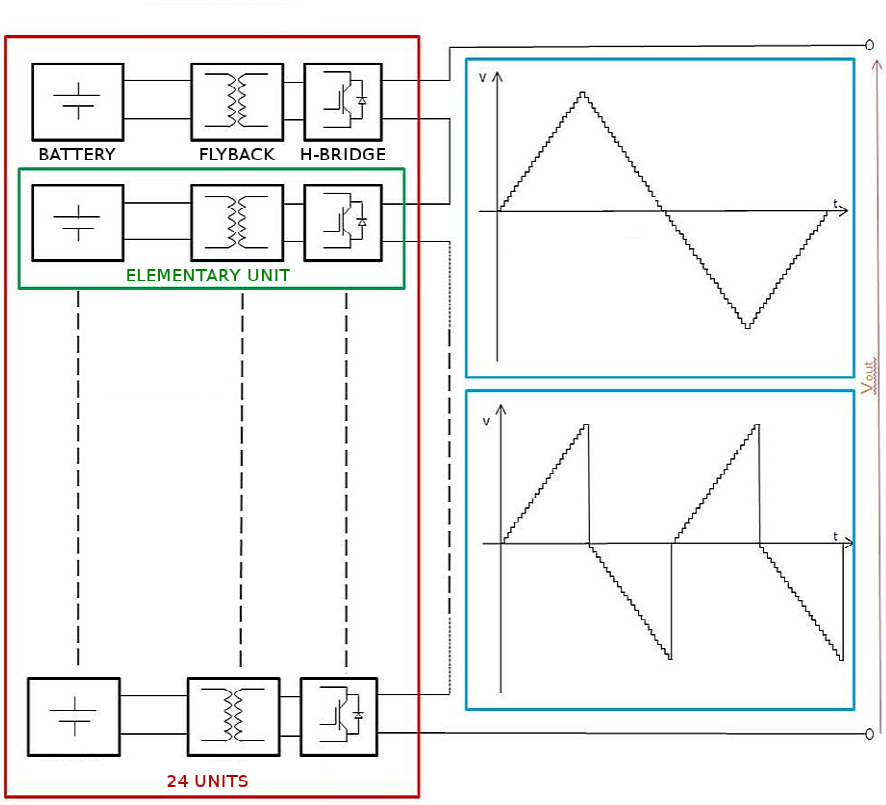

Figure 2.1 Schematic view of the multilevel converter

2.2 Batteries and Isolation

Apart from the many advantages that a cascaded topology has, there is a very well known and documented issue when applying these circuits. It is graphically depicted in Fig. 2.2

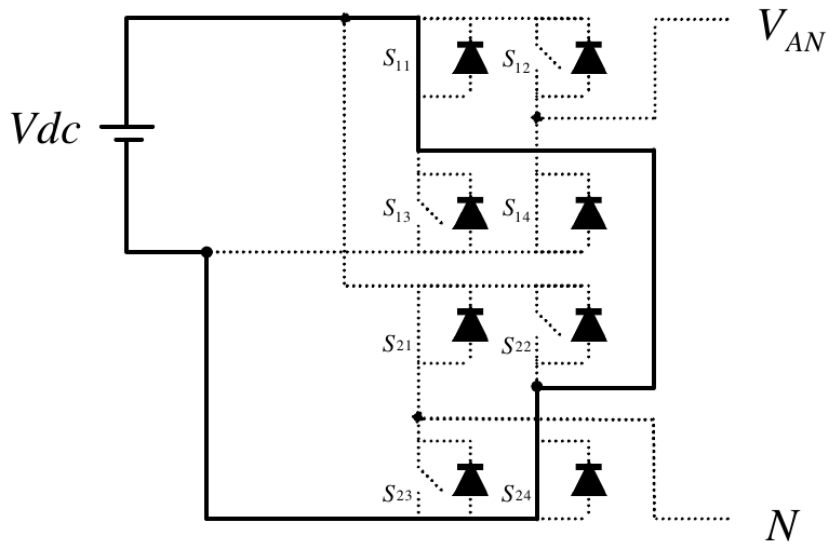

Figure 2.2 Short-circuit situation

If we assume a 5 level cascaded H-bridge, it is composed of two elementary H-bridge units as seen in the picture. The output voltage is V_{AN} and both the two parts of the circuit are connected to the same power supply source V_{dc}. When switches S_{11} and S_{24} are ON at the same time a direct path to the ground is formed, i.e. a short circuit situation happens. In a topology like this one this event is not correlated to a fault situation and can happen during regular operation. Thus, it should be taken into account and definitive measures should be adopted in order to prevent the triggering of this event.

The most effective way of dealing with this problem is to keep the power supplies of each H-bridge separated and isolated. A common solution is to use a transformer with multiple windings on the secondary side that supply each H-bridge and one common primary winding connected to the main power supply.

This solution would not be optimal if applied to the presented multilevel converter. Each elementary unit is at floating potential with respect to the ground. Due to the high output voltage of the multilevel the units can also reach high voltage difference to the ground. Thus if a single power source is to be used, i.e. the primary winding of the transformer, high isolation levels have to be provided between each unit and the primary. Consequently an isolation of almost 15 kV should be guaranteed between all the windings of the transformer. Although feasible, this kind of isolation is common practice for high voltage systems, it would have been an unpractical fix to the issue. The transformer would have been big in size and highly inappropriate for the purpose of this project.

As such in order to provide galvanic isolation between the power supplies of each stage the most suitable solution was to use batteries. Therefore each H-bridge is independently supplied by a 12 V – 4000 mAh lead acid battery. Lead acid batteries provide robustness and reliability as well as ease of charge. The use of batteries solves both the isolation and the short-circuit problems. Another advantage of using batteries is the portability of the whole multilevel inverter. No connection to a mains power supply is needed and the presence of a heavy transformer is avoided.

2.3 The Flyback Converter

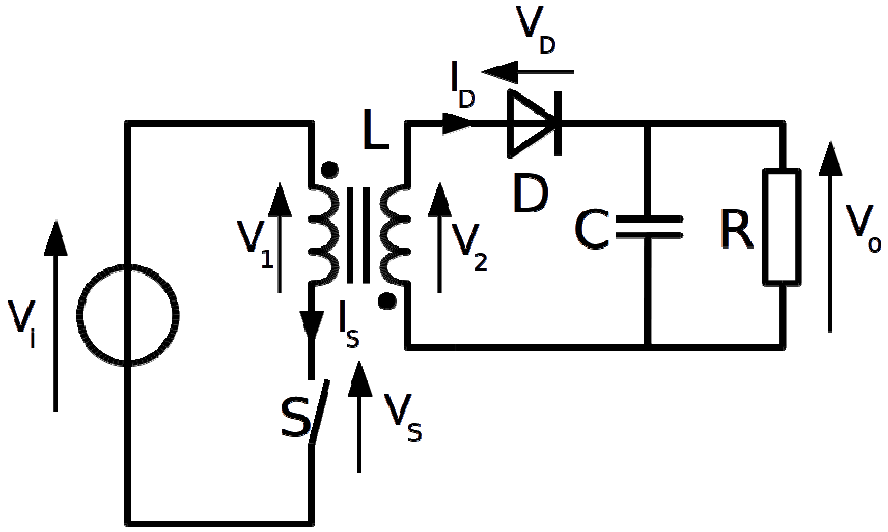

Figure 2.3 Flyback converter

The flyback converter is derived from the buck-boost topology of dc/dc converters. In fact it is an isolated version of that scheme because it incorporates a transformer which provides galvanic isolation between the input stage and the output. Apart from the isolation the flyback converter has a number of advantages that make it one of the most widely used dc/dc topologies. In comparison to other isolated converters like the forward or the push/pull scheme it is much simpler. It is a robust topology and few components are needed to build one (only one switching device and no output inductor). Finally with the use of separate windings the secondary stage can be split into different outputs. As it will be shown this final convenience has been significantly useful in the development of the dc bus for the elementary inverter boards.

2.3.1 Operation of the Flyback

While S is ON current flows throw the primary inductance of the transformer and its value rises linearly. It reaches the highest value I_{pk} just before S is switched off: When S is switched off all the magnetic energy stored on the primary side is transferred to the secondary due to the fact that the current flowing through the inductance cannot turn to zero instantly when the circuit is opened. Flybacks can be operated in two modes:

- Continuous mode
- Discontinuous mode

The first one also called “incomplete energy transfer” happens when only part of the energy stored in the transformer at the end of an “ON” period is transferred to the output and some of it remains in the transformer at the beginning of the next “ON” period. The second one also called “complete energy transfer” happens when all of the energy stored in the transformer during the “ON” period is transferred to the output.

The two operating modes have a quite different small signal transfer function. In particular the discontinuous mode has a single pole transfer function while the continuous has two poles and a right half plane zero which can cause instability if the flyback is operated at high frequencies. In order to avoid such situation the discontinuous mode has been selected as the desired mode of operation.

Figure 2.4 depicts the typical waveforms of a flyback operating in discontinuous mode. As said when the switch is turned OFF current starts circulating on the secondary winding.

This happens when the primary current has reached its top value and the switch is opened. During the “OFF” period the output diode is directly polarized and the capacitor is charged.

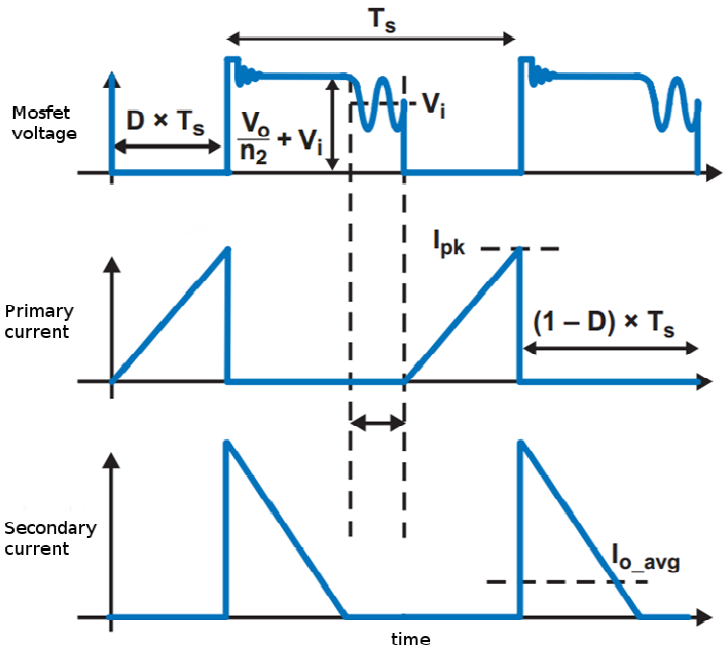

Figure 2.4 Flyback waveforms

The output current decreases linearly from a given maximum value. An overshoot on the drain-source voltage of the mosfet is evident when the switch is turned off. This event happens because the reflected voltage from the secondary is added to the already existing input voltage.

This overshoot must be controlled in order to prevent damage to the mosfet. This is usually done through the use of clamp circuits that limit overvoltages. Finally looking at the voltage waveform two different ringing frequencies can be observed. The first one that happens after the switching is due to the resonance between the leakage inductance of the transformer and the leakage drain-source capacitance of the

mosfet. The second ringing is due to the magnetizing inductance and the drain-source capacitance. Both of these problems can be solved by the use of appropriately sized snubber circuits.

2.3.2 Designing the Flyback

The most important part of a flyback converter is the transformer. A careful study has to be made in order to avoid saturation, minimize losses and maximize efficiency. Ferrite cores are usually the best option for this type of devices because they provide minimum loses at high frequencies, which is exactly the case of a flyback converter.

At the beginning of the design the known parameters are:

- The supply voltage Vi,
- The output voltage Vo,
- The ouput current Io,
- The tolerable voltage ripple ΔVo.

The first step is to set the maximum duty cycle D in order to guarantee the discontinuous operation mode but also to limit the maximum Vds voltage which the mosfet will be able to sustain. In this case

$$D^{max} = 0.45$$

Thus the maximum value of Vce is given by

$$V_{ce}^{max} = \frac{V_i}{1 - D^{max}}$$

The the maximum value of the mosfet current is then calculated

$$I_c^{max} = \frac{2P_o}{\eta V_i^{min} D^{max}}$$

Where *Po* is the expected output power and *η* is the efficiency. A typical value for η is 0.7. The primary inductance is

$$L_1 = \frac{(V_i^{min} \cdot t_{on}^{max})^2 \eta}{2T_{sw} P_o}$$

Where T_{sw} is the switching period and t_{on}^{max} is the maximum ON time of the mosfet. In order to avoid core saturation an air gap has to be inserted in the core. The value of the air gap is given by

$$G_{air} = \frac{L_1 I_c^{max}}{B^{max} A_e \mu_o}$$

Once air gap is introduced the reluctance of the magnetic circuit can be approximated to the one given by the air gap. In particular the parameter A_l is defined as

$$A_l = \frac{A_e \mu_o}{G_{air}}$$

A_l is the inverse of the reluctance. Once the core values are defined the necessary primary winding turns can be calculated

$$N_1 = \sqrt{\frac{L_1}{A_l}}$$

Finally the secondary windings are given by the relation

$$\frac{N_1}{N_2} = \frac{(V_i^{min} - V_{ds}^{on}) \cdot \eta T_{sw}}{(V_o + V_{fd}) \cdot (T_{sw} - \eta T_{sw})}$$

Where V_{fd} is the output diode forward voltage drop.

Following the above procedure the turns per winding were calculated. In particular for a 12 V input voltage supply with an output voltage of 600 V the secondary winding has been split into 6 secondaries that are series connected.

This design choice was done in order to have a more efficient system and to use low voltage components on the secondary windings. The primary winding is made of 2 turns and each secondary has 19 turns.

A complete SPICE simulation of the developed flyback converter has been implemented using the LTSpice software.

Fig. 2.5 shows the PSPICE model of the flyback converter. The implemented circuit is an exact copy of the circuit that was eventually realized. Also, the electrical values of all components correspond to the real for the tweaking of which the simulation has been very useful.

Fig. 2.6 shows the runtime graph of the output voltage. It is the sum of 6 flyback windings that have an output voltage of 100 V. Therefore a 600 V final output is generated which forms the DC bus for the DC/AC stage.

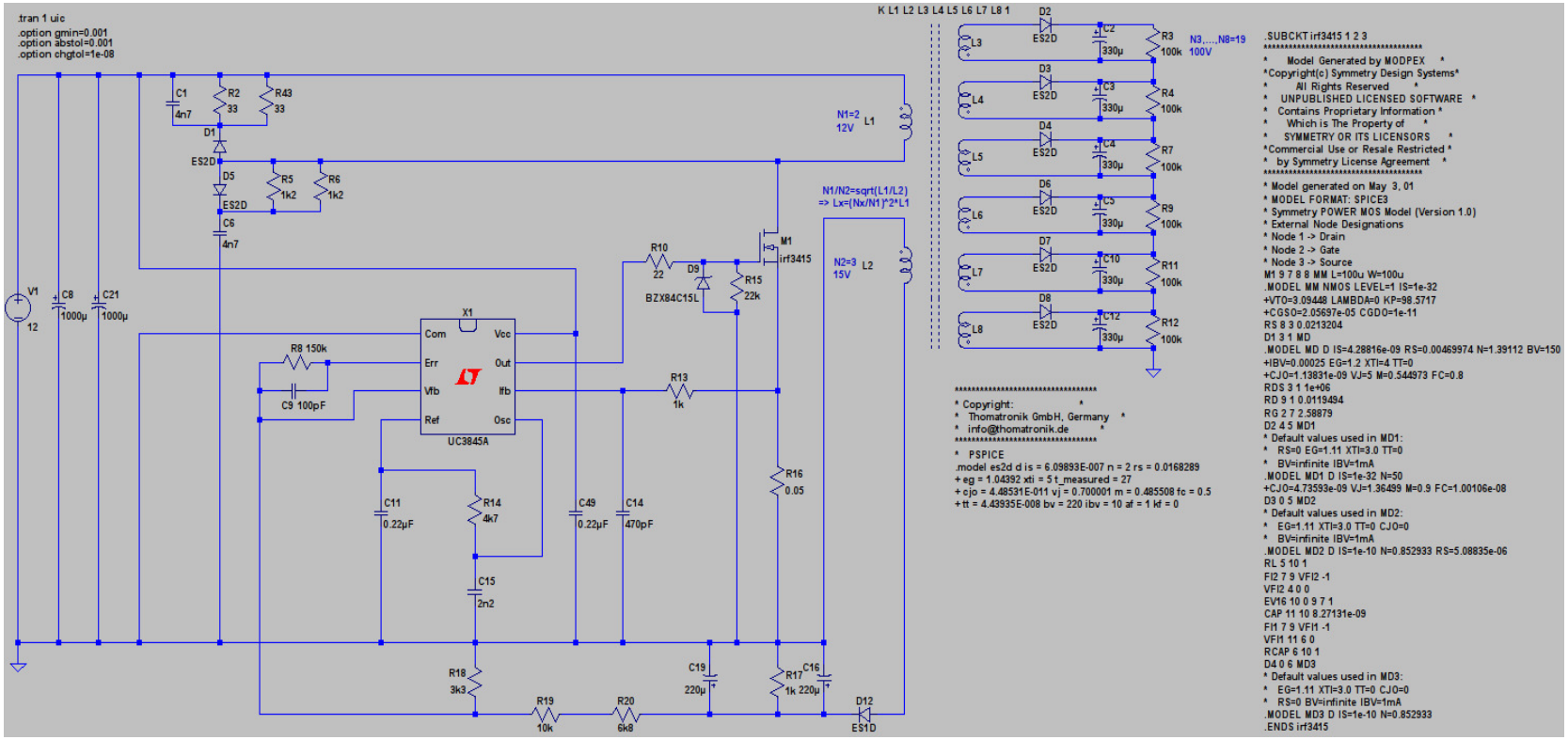

Figure 2.5 Flyback LTspice schematic

Figure 2.6 Simulated output voltage of the flyback

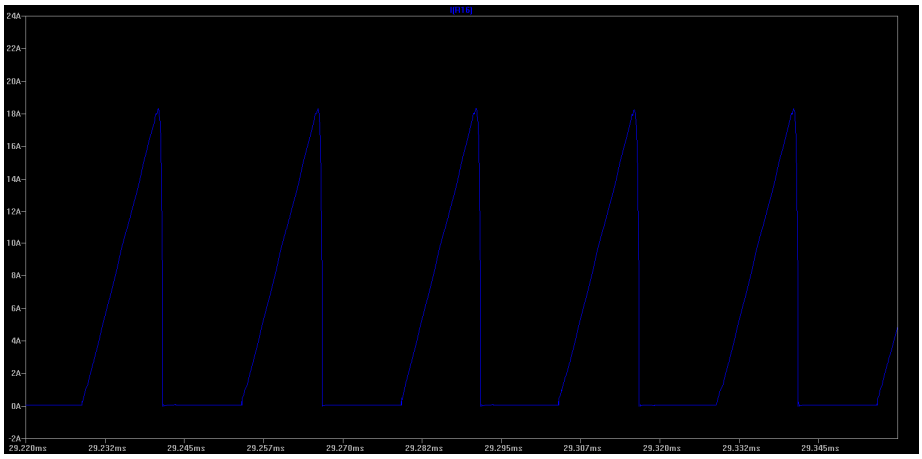

Figure 2.7 Simulated current at start phase

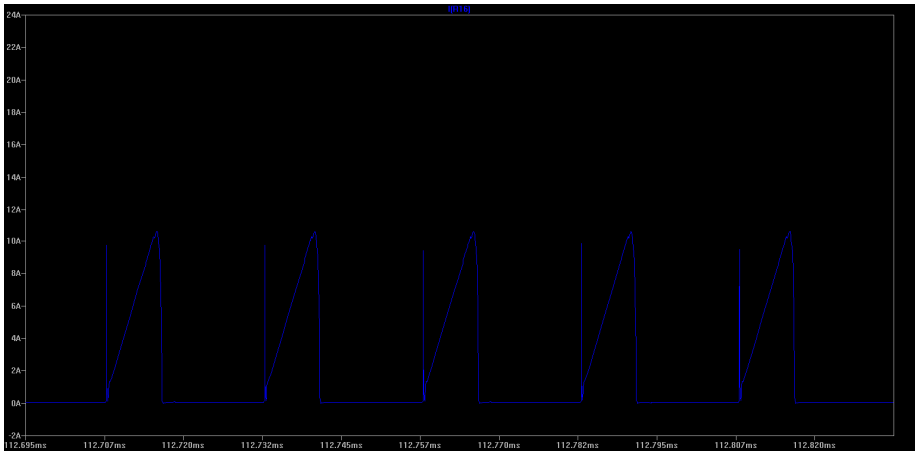

Figure 2.8 Simulated current end phase

Fig. 2.7 and Fig. 2.8 show the current in the mosfet during two different time frames. The first one happens when the output voltage is still rising fast. It can be seen that the flyback is trying to provide the maximum power to the load. The duty cycle is almost 50% and the current peaks at its top value. In the second figure the output voltage is rising slower, the voltage is reaching the desired level and the requested power from the mosfet is decreasing. Thus the peak value is decreased and the duty cycle is significantly lower than 50%.

2.4 The DC/AC stage

The final part of the elementary unit is the DC/AC converter. In order to keep the physical size of the unit as compact as possible an integrated power module was used. These modules are practical because they incorporate a three phase inverter based on IGBT technology as well as the driving circuit. Dedicated IC for self-protection against over-current, undervoltage of control power supply and over-heating is also included.

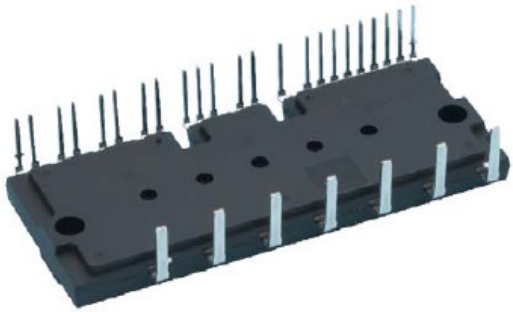

Figure 2.9 Integrated power module

In particular the module that was used to implement the DC/AC stage of the elementary unit is the model PS22A74 by Mitsubishi Semiconductors which has the following specifications:

- Three phase 5th generation IGBT
- 1200 V (Collector-Emitter)
- 15 A
- 20 Mhz max operating frequency

As it can be noticed the module is three phase though the multilevel inverter is single phase. Therefore in order to form

an H-bridge only two legs of the integrated three phase circuit are used. The third leg can be used as a backup.

2.5 PCB Overview

The elementary unit of the multilevel inverter has been implemented on a single printed circuit board that comprises of the step-up stage provided by the flyback converter and the inverter stage provided by the integrated module. The control of the power mosfet on the primary side of the transformer is realized with the use of current mode PWM controller. The power supply for the controller is provided by the battery. Two feedback loops are present. A current sensing circuit that goes directly to the controller and a voltage sensing circuit. The later one has been implemented through the use of a dedicated secondary winding that provides a scaled measure of the voltage on the output secondaries.

The working frequency of the flyback is set by the PWM frequency generated by the controller and it is 80 kHz. The PWM has a maximum duty cycle of 50% in order to guarantee the discontinuous mode of operation of the flyback. During operation the maximum voltage on the primary is 20 V. In order to protect the transistor a RCD clamp circuit is present as well as a snubber circuit.

The transformer has been designed in order to sustain 3 kV voltage potentials between the primary and the secondary windings. This is more than enough to guarantee galvanic isolation between low voltage given by the battery, 12 V, and high output voltage which is 600 V. Apart from the primary winding and the voltage feedback winding there are a total of 7 secondary windings. As said, the output voltage

secondary which provides the 600 V has been split into 6 secondary windings of 100 V each. These secondaries have been series connected to generate the high output voltage. Finally an auxiliary winding is present in order to provide low voltage power to circuits needing 5 V and 15 V.

Name	# turns	Voltage
Primary	2	12 V
Feedback	3	~ 15 V
Aux	6	~ 30 V
Out 1	19	~ 100 V
Out 2	19	~ 100 V
Out 3	19	~ 100 V
Out 4	19	~ 100 V
Out 5	19	~ 100 V
Out 6	19	~ 100 V

The flyback transformer's core has an air gap of 1 mm. The air gap is necessary in order to prevent the core from saturating because of the high working frequency. The air gap width has also been carefully minimized for the best possible efficiency.

The 600 Vdc output of the flyback converter forms the dc bus of the integrated inverter module and it is connected on pins P-N. In order to control the each elementary safely, galvanic isolation had to be guaranteed between the low voltage control electronics and the high voltage generated on the output of the inverter. Fiber optics were used in order to implement this isolation. As seen in Fig. 2.11 two fiber optics receivers are used. As a safety precaution and in order to ease the control dead times have been hardware implemented on board.

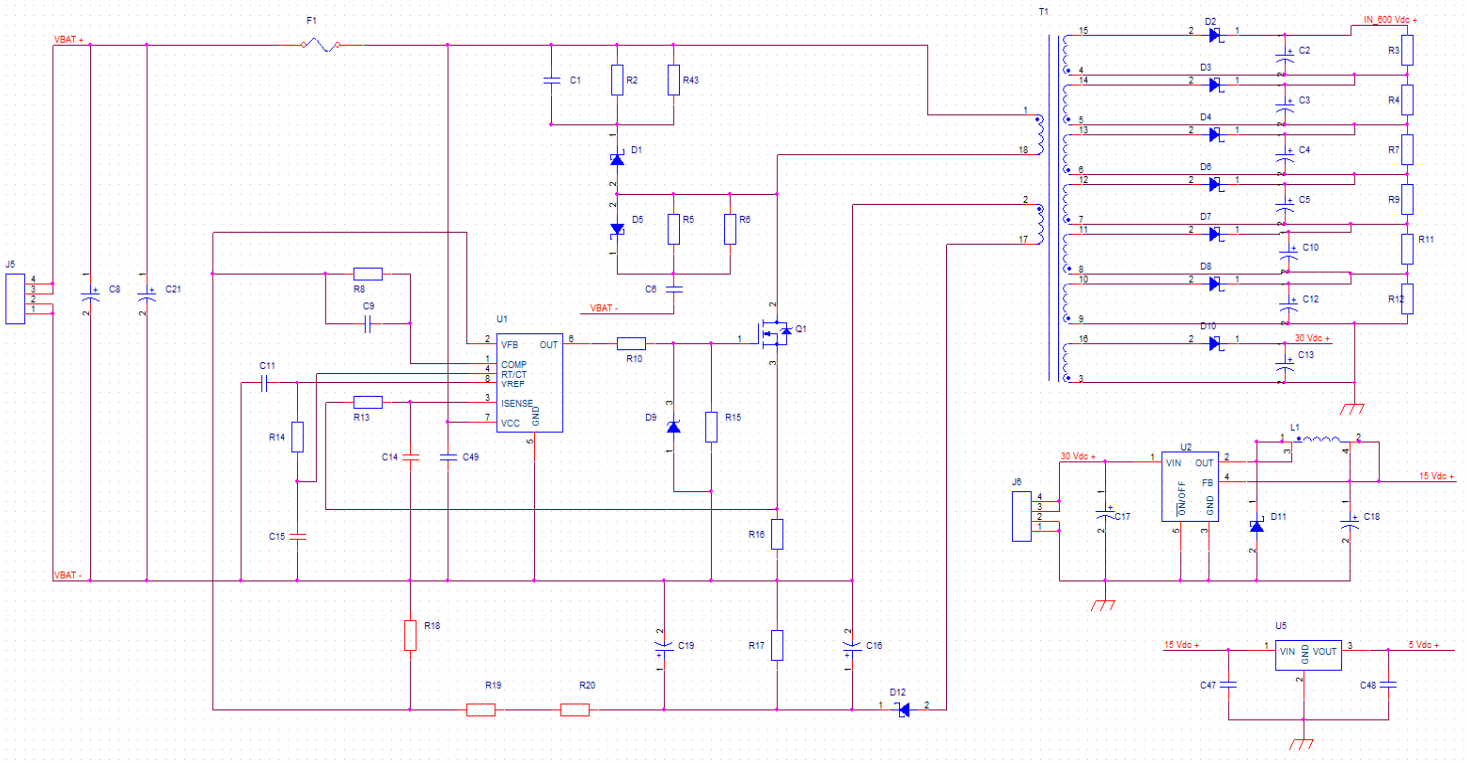

Figure 2.10 Orcad schematic of the flyback part

The two control signals propagate through a 6 input inverting buffer that generates two couples of negated signals, one couple for each inverter leg. Through the use of a pull-up resistor and a capacitor the signals are appropriately delayed. Finally a Schmitt trigger sharpens the signal edges and stabilizes the delay which is of 3 us.

The control signals are then fed to the integrated driving circuits. As said the module is composed of three legs but only two of them are being used. Part of the necessary auxiliary circuit are the bootstrap capacitors for the high IGBTs. These circuits as well as the fiber optics receivers have to be power supplied with 15 V and 5 V respectively. The secondary winding on the flyback converter that outputs 30 V is used to power these circuits.

Making use of low voltage components has led to a limited sized board. The final PCB is square shaped at 14x14 cm.

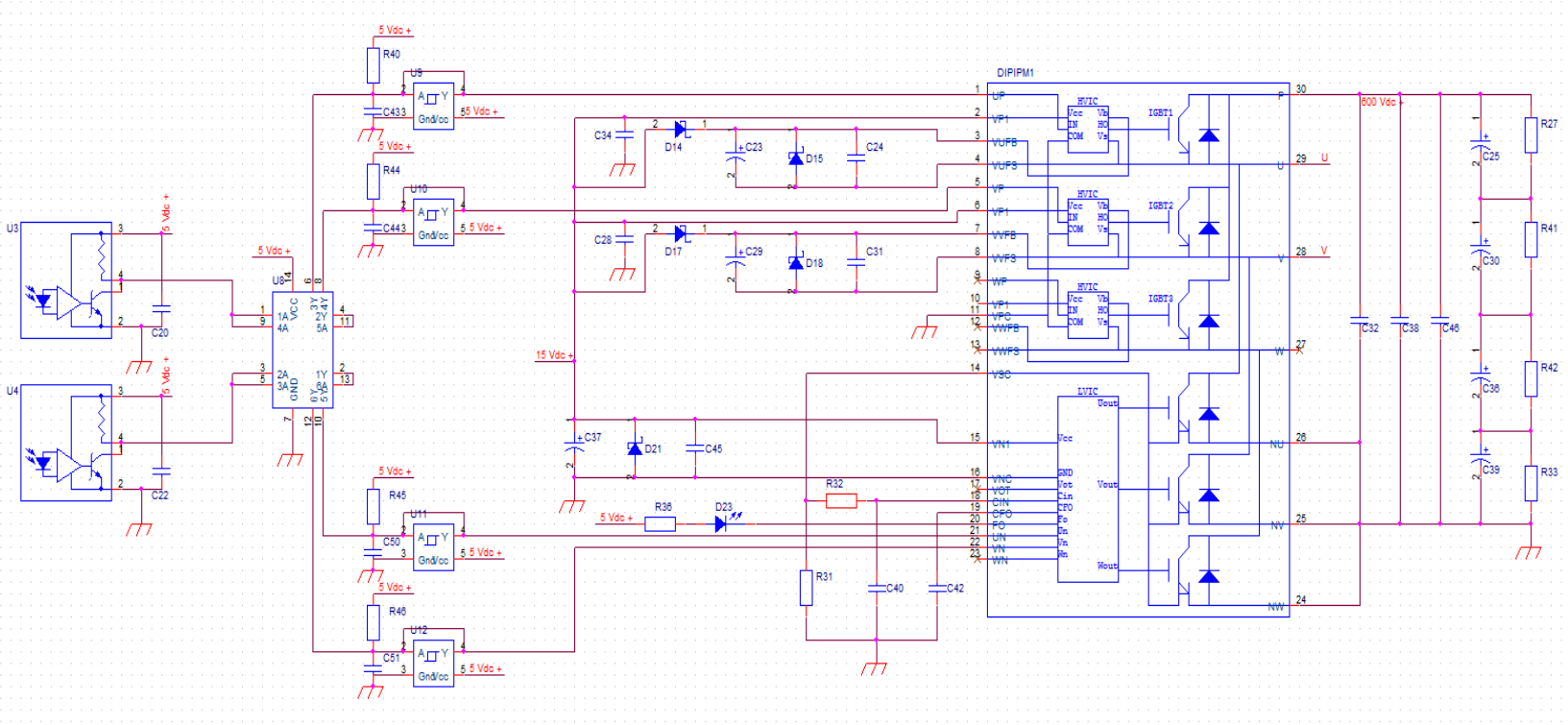

Figure 2.11 Orcad schematic of the inverter part

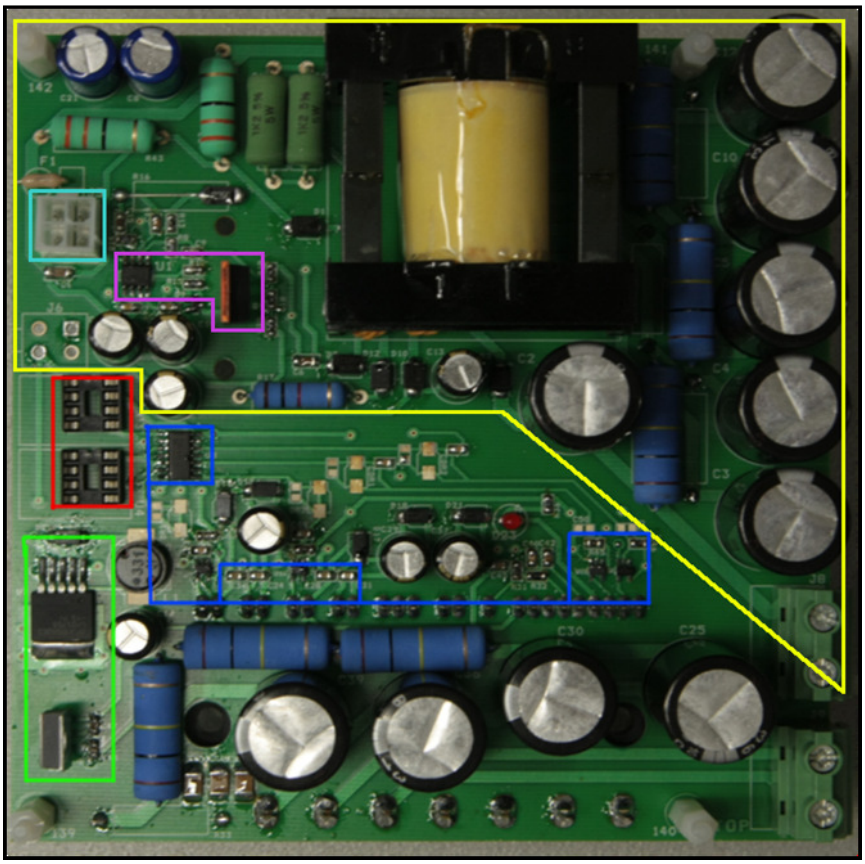

Figure 2.12 Manufactured elementary unit: Top

Figure 2.12 illustrates a realized elementary unit. The board is clearly divided into two marco regions. The higher part surrounded by the yellow border is the flyback converter while the lower part of the board is the DC/AC stage.

The main parts of the flyback are:

- The battery input connector (cyan)
- The transformer
- The Mosfet and the pwm regulator (purple)
- The two low voltage regulators (green)
- The placing for the Fiber optics (red)
- The dead time generation circuit (blue)

Fig. 2.13 shows the lower view of the PCB where the integrated inverter module is housed.

The elementary units have been stacked in piles. The connections between each board has been done with the use of common cables and with a series connected fuse.

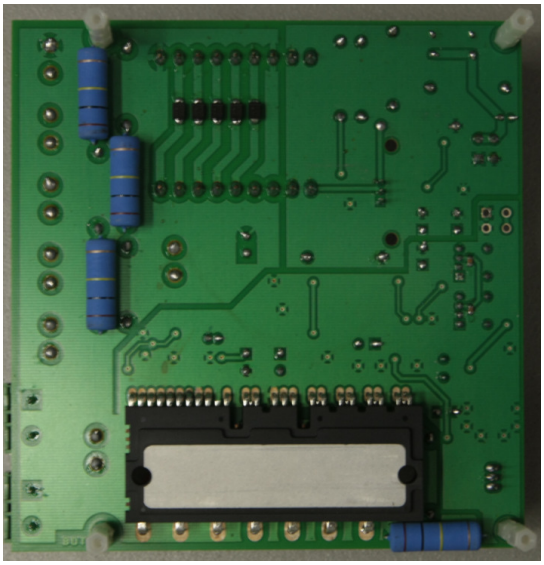

Figure 2.13 Manufactured elementary unit: Bottom

Figure 2.14 Stack of 8 elementary units

Figure 2.15 Complete system

All the boards have been split into 3 stacks of 8 PCBs. This was possible due to the modularity of the inverter and it was done for using it for three phase applications too. 24 switches had to be installed in order to activate each battery and guarantee isolation. The batteries are also attached to external plugs that are used when recharging the inverter.

Finally as it can be seen the control unit is placed on on top of the three pvc cases. 48 fiber optics travel from the control board to all elementary units.

Chapter 3

SYSTEM IMPLEMENTATION: SOFTWARE AND CONTROL

3.1 Control Method

The multilevel inverter is composed of 24 PCBs. Two control signals are required on each board thus a total of 48 signals have to be generated and transferred to the inverter.

All typical control methods for multilevel converters are based on modulation techniques. A very popular method mainly used in industrial applications is the carrier-based sinusoidal PWM that uses phase-shifting to reduce harmonics in the load voltage. Another alternative is the Space Vector Modulation strategy as well as the Space Vector PWM.

Each modulation method has its own advantages though all of them share a common drawback which is that as the number of levels increases the complexity of the control implementation through digital means increases dramatically. With respect to that consideration, a 49-level inverter poses a big challenge.

In order turn the large number of levels from a disadvantage point to an advantage a totally different approach was chosen. The proposed technique is based on a microcontroller unit that generates all 48 signals for the multilevel. Each signal directly sets the state of the elementary unit in accordance with the other units. Through the use of appropriately set delays the switching instants for each IGBT is

controlled. Modulation is not needed as the large number of levels provides a good resolution detail on the output voltage.

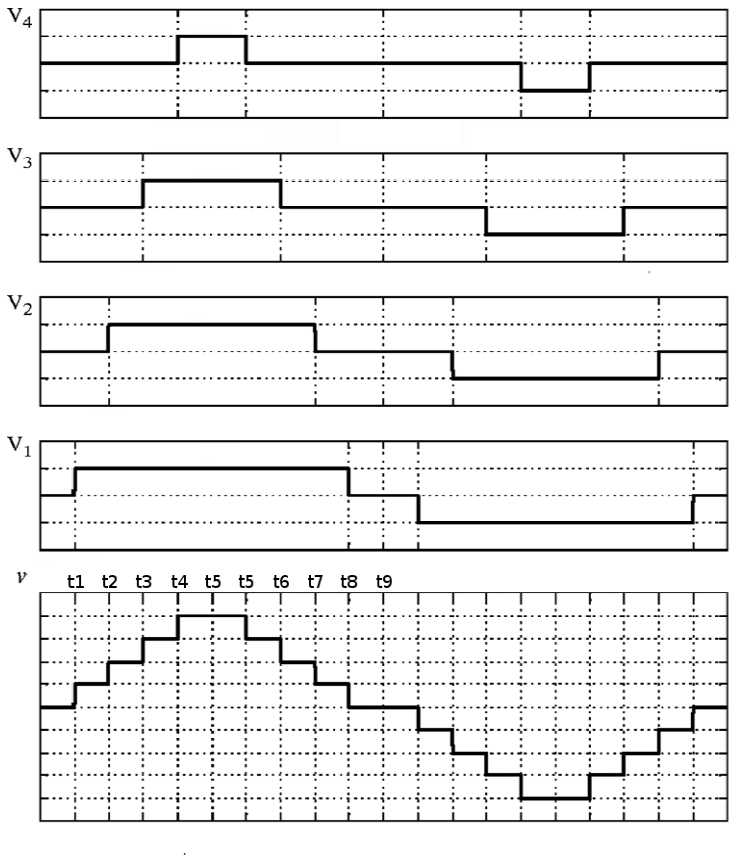

Figure 3.1 Multilevel waveform

Let us assume the already showed 9-level waveform, Fig. 3.1, then the control method can be easily explained. This waveform is composed of 4 separate elementary units that provide a given and same to each other output voltage. The control method works on the triggering instants t1, t2 , etc. and on the duration of the applied voltage on each elementary unit. For example voltage V1 has to be set to the positive output voltage at t1 and this event should last until t8 while V4 should trigger at t4 and remain high until t5.

This example shows how the voltage resolution of the output waveform for 9 levels is low but scaling this control method to a 49-level inverter makes this solution much more reasonable. The 28,8 kV peak to peak output is divided into 600 V steps, i.e. ~2% of the total voltage.

3.2 The control unit

The mentioned control method has been implemented with the use of a microcontroller board. High processing power is not a strict requirement for the control unit. However the number of available digital I/O is very important because 48 signals have to be generated. The ATmega1280 8-bit microcontroller from ATMEL was chosen which provides 54 digital I/O. The Arduino open source platform was used to program the MCU which physically resides on the Arduino board.

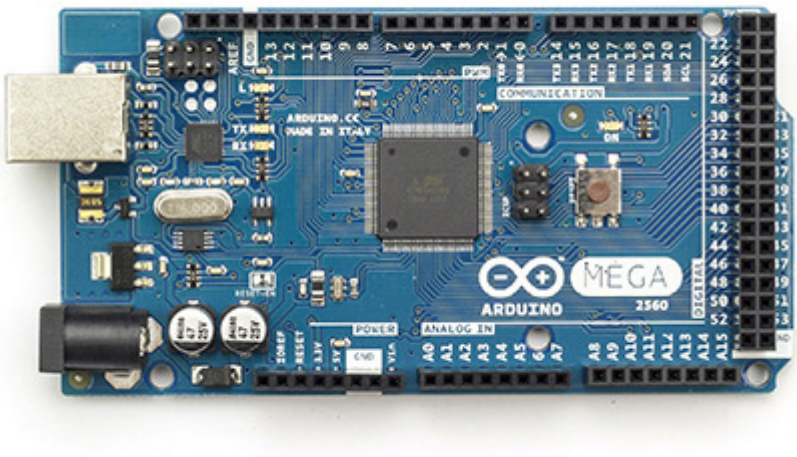

Figure 3.2 Arduino MCU

Included with the Arduino is the integrated development environment (IDE) that serves as a programming and compiling tool for the MCU. The programming can be done in C language or in Assembly. The control algorithm is based on the setting of firing instants and delays. As such it is very sensitive to timing variations that can be introduced by software loops or interrupts during the sequential execution of the program. In order to prevent unexpected behaviour during runtime the program had to be written in Assembly language avoiding loops and disabling interrupts.

What follows is an example of the code that runs on the MCU. In particular the first 4 steps of a triangular waveform at 5 kHz are shown:

```
void setup(){
  DDRA = B11111111;
  DDRB = B11111111;
}

void loop(){
  cli();
  PORTA=B00000001;
  PORTB=B00000000;
  delayMicroseconds(4);
  PORTA=B00000011;
  PORTB=B00000000;
  delayMicroseconds(4);
  PORTA=B00000111;
  PORTB=B00000000;
  delayMicroseconds(4);
  PORTA=B00001111;
  PORTB=B00000000;
  delayMicroseconds(4);
```

Like a normal C program the functions `setup()` and `loop()` have to defined. In the setup the I/O registers A and B are set as outputs by activating the all the bits. Because only 16 bits are set, i.e. two registers, it can be deduced that this code refers to eight elementary units as two signals are needed to drive each unit.

The instruction `cli();` is necessary to disable interrupts inside the loop. This is needed in order to have more stable signals and avoid jitter effects that affect the output signals of the MCU when interrupts are enabled.

The instruction `PORTA=B00000001;` sets the state of the respective signals on register A. As it can be seen be the code in order to generate a triangular wave the outputs have to be progressively activated. Note that not only active signals have to be set but also the 0s have to be reset each time in order to avoid mistakes that have been noticed during runtime.

Finally the `delayMicroseconds(4);` sets the delay between each voltage step in the multilevel staircase. The minimum delay that can be set is 1 us.

As said low level language has been used in order to avoid unnecessary delays due to high level commands' execution during runtime. For example it has been measured that the typical delay introduced by `PORTA=BXXXXXXXX;` instruction is about 65ns while the respective high level command introduces a delay of more than 400ns.

3.3 Simulations

A simulation of the complete multilevel inverter has been developed in order to evaluate the expected behaviour when the system is connected to a load. A plasma actuator can be roughly simulated as a series RC circuit. In particular a resistor of 1kΩ and a capacitor of 10pF were set as the load. The simulation was developed in Matlab – Simulink. Fig 3.3 depicts the overview of the the model. The elementary units have been divided into three blocks that comprise of eight units, just like the real implementation.

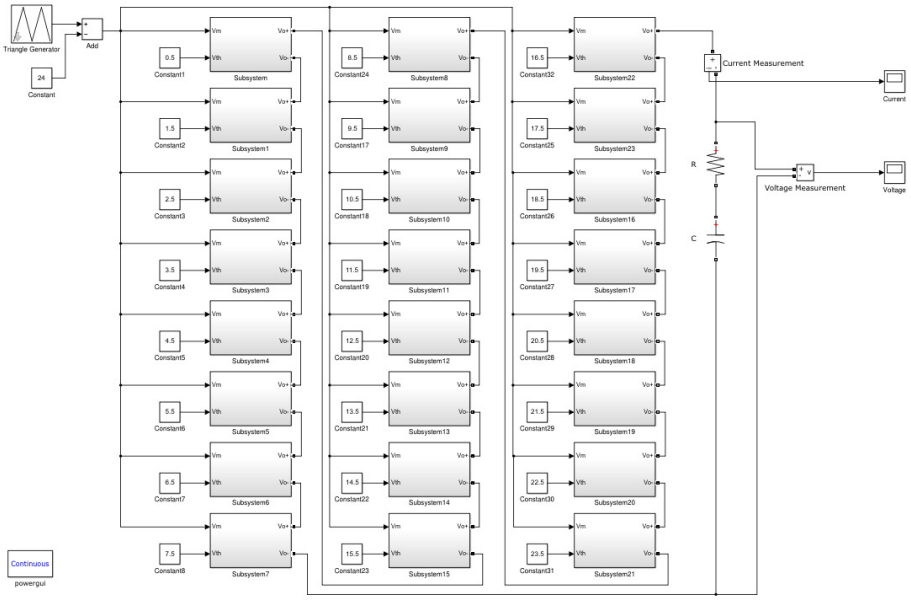

Figure 3.3 Simulink model of the total system

The output voltage is controlled by an input reference signal. Arbitrary waveforms can be generated. In this example a triangular waveform at 10 kHz was used. The value of the reference signal ranges between -24 to 24. To each unit a threshold value is assigned ranging from 0.5 to 23.5 with steps

of 1. For example the first unit (top left corner) the threshold value is set to 0.5. The second unit takes a value of 1.5 and by applying the same principle to all units the last one receives a threshold value of 23.5. Fig. 3.4 shows the first positive quarter period of the triangular wave with the respective triggering instants.

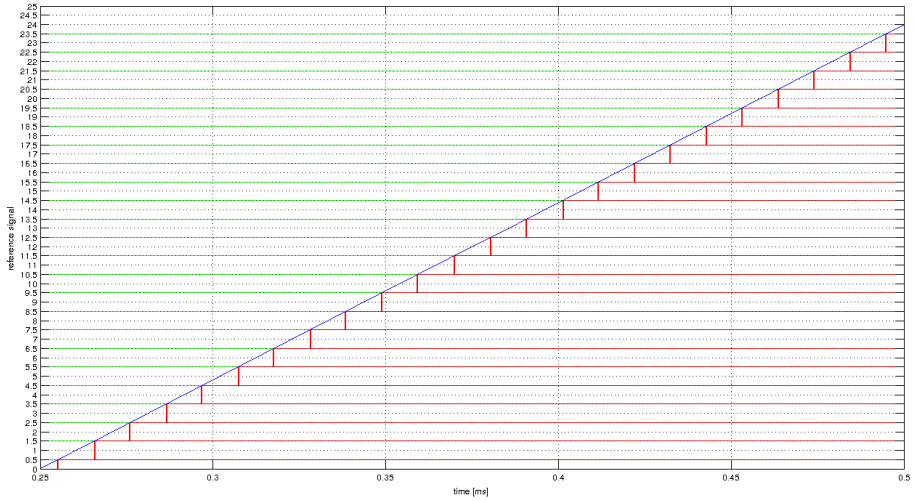

Figure 3.4 Waveform formation

The elementary unit block is composed of two parts. The first one is called “Driver”, Fig. 3.5, and it is responsible of comparing the reference signal value with the given threshold value.

A detailed view of the driver, Fig. 3.6, shows that in order to take into account the negative part of the reference signal, i.e. the output waveform, the comparison is done both with a positive value of the threshold *Vth+* and with a negative value *Vth-*. The converter block is just used to transform numerical values to signals *Vmq1* and *Vmq3*.

Vmq1 and *Vmq3* are the control signals that are fed to the second block that composes the elementary unit which is the “H-bridge” shown in Fig. 3.7. The H-bridge can have three possible states:

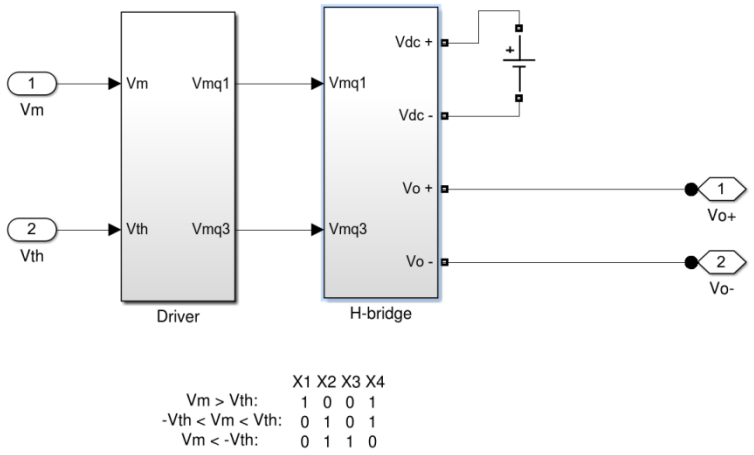

Figure 3.5 Elementary unit model

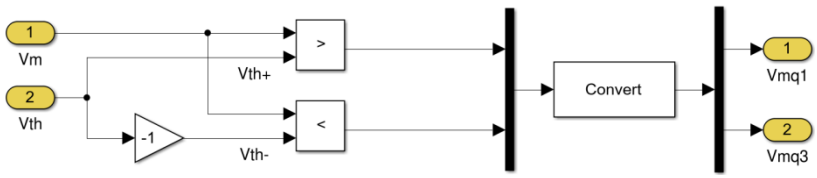

Figure 3.6 Driver model

1. Q1,Q4 closed and Q3,Q2 open when the reference signal is above the threshold and the output voltage is positive (600 V).
2. Q3,Q2 closed and Q1,Q4 open when the reference signal is below the threshold and the output voltage is negative (-600 V).
3. Q2,Q4 closed and Q1,Q3 open when the reference signal is between the positive and the negative values of the threshold and the output voltage is 0. Basically the unit is by-passed.

The final 49 level output voltage is depicted in Fig. 3.8.

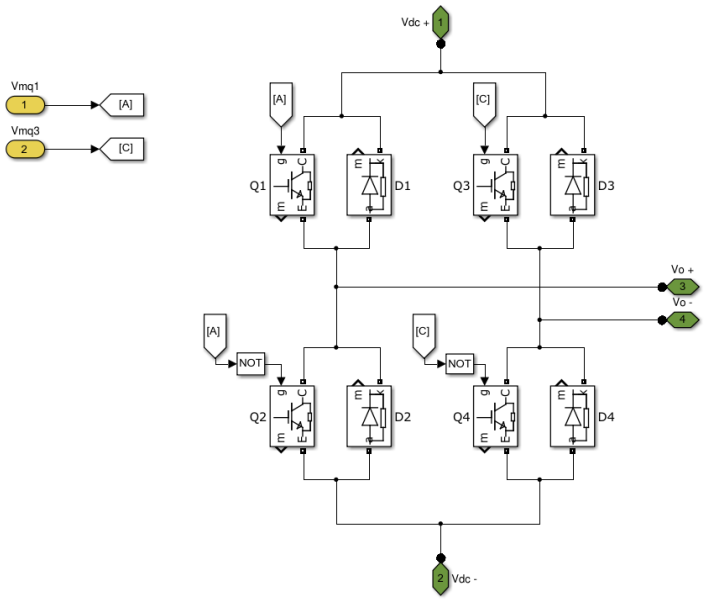

Figure 3.7 H-bridge model

As it can be seen the voltage goes from -14,4 kV to 14,4 kV and all elementary units are used. The reference waveform is perfectly replicated on the output.

Fig. 3.9 shows the current. Due to the capacitive nature of the load the current has a totally different waveform than that of the voltage. In fact it is a series of spikes. Between each spike the current goes to zero. As it will later be shown this is a very realistic behaviour of a plasma actuator load. The current spikes happen in correspondence to the voltage steps, either positive or negative, the polarity obviously follows that of the voltage. This fact shows that elementary units conduct current in a discontinuous way and only for a short period of time after switching.

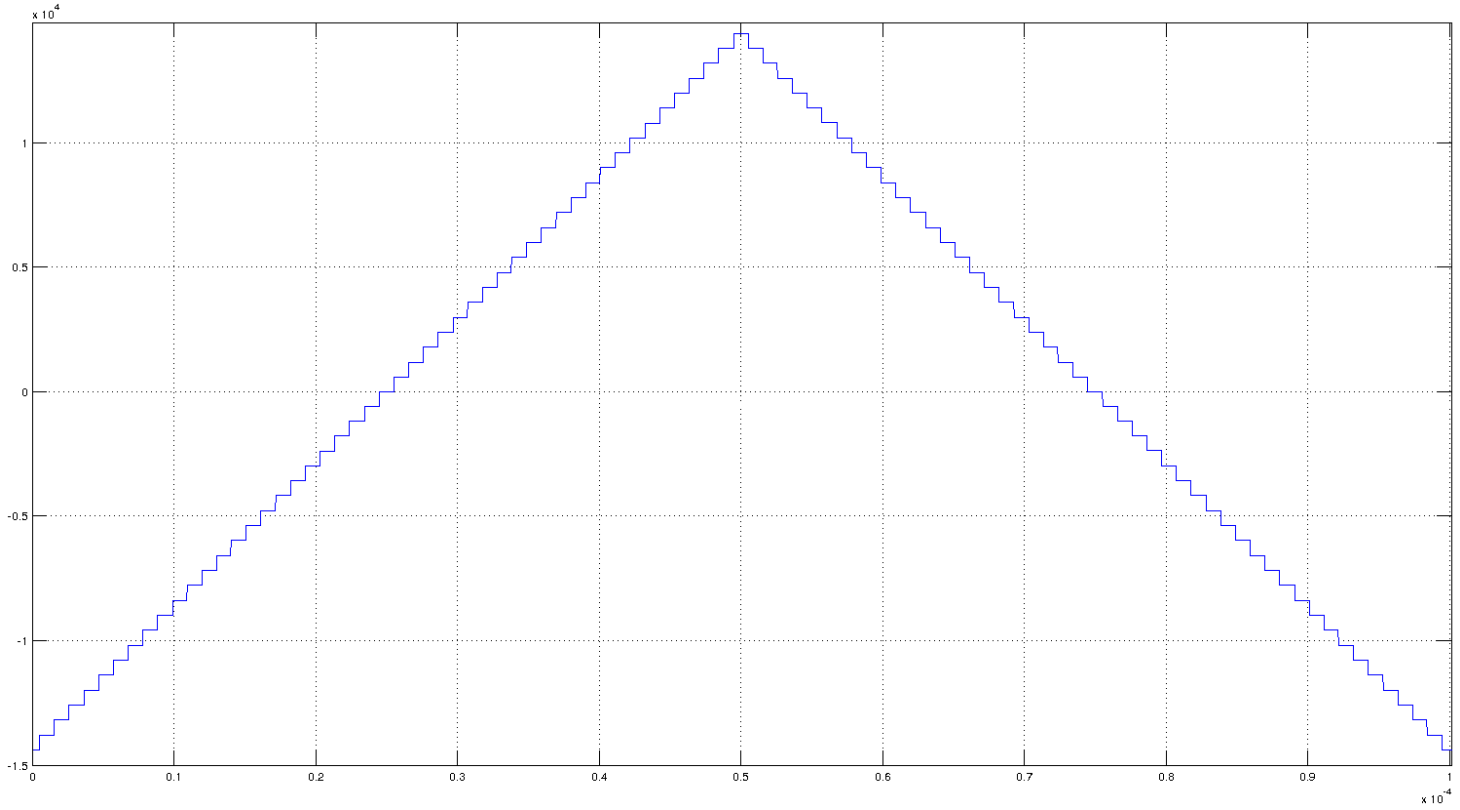

Figure 3.8 Simulated output voltage waveform

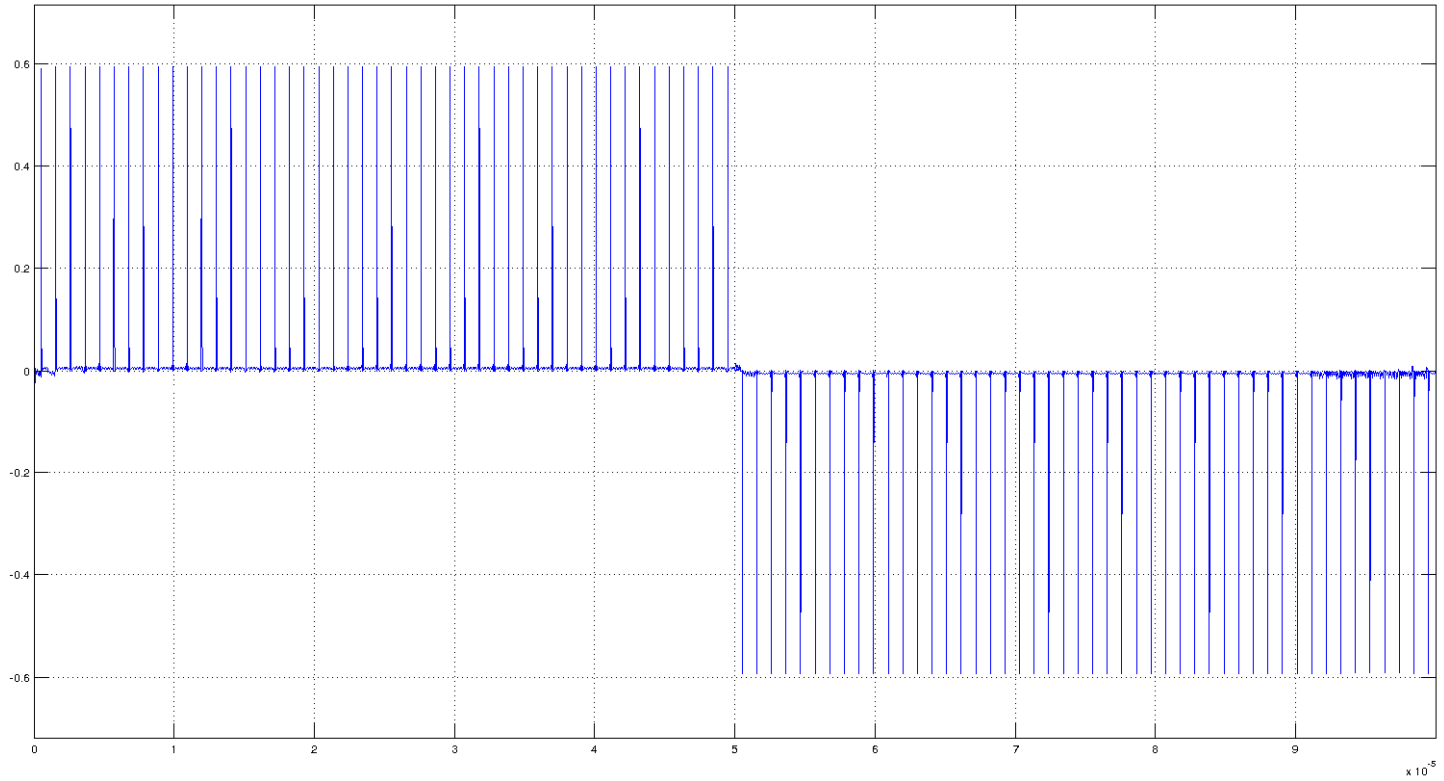

Figure 3.9 Simulated output current

3.4 Input power balancing

It should be clear by now that if the implemented control method was a strict copy of the previously showed simulation an unbalance on the use of the modules would happen. It is evident that if the thresholds of each unit are statically set some units “work” more than others. Fig 3.10 shows the level voltage of the first unit V1 and that of the last unit V24 which correspond respectively to the lowest threshold value and to the highest. Only a few cycles are needed in order to show that the unit that has the lowest threshold, V1, is active for a longer period of time that V24 which has the higher threshold and therefore activates only when the reference signal peaks at its limits.

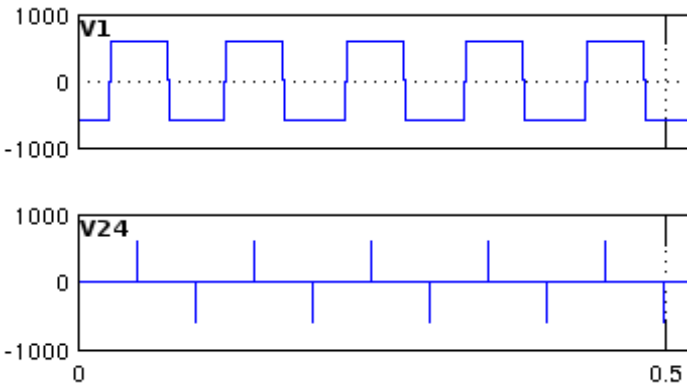

Figure 3.10 Detailed view of V1 and V24

Evidently the unit with the lower threshold conducts current while active for much longer time than the one with the highest threshold. Thus the unit that corresponds to V1 provides more power to the system than the unit that has V24 voltage. For a multilevel inverter that it is based on batteries this means

that the battery connected to the first unit will discharge faster than the one connected to the second unit.

This can be a problem for two reasons. First of all if the batteries are discharged in different manner the use of the multilevel before a recharge cycle is bonded to the battery life of the lowest threshold unit. Thus the system could stop working properly only due to a couple of discharged batteries while the rest could still function. This leads to the second problem which has to do with the expected lifetime of the batteries. The optimal way of charging requires the batteries to be at the same level of charge. In this condition this would be problematic.

In order to solve this issue a couple of more advanced control methods were simulated, with one of them actually being implemented on the real system. These algorithms are an attempt to render the discharge of the batteries homogenous.

3.5 Cycling Levels

The first control method is also the one that has been implemented on the real system. It is an open loop control method. The idea is to vary the thresholds of the units in order to have them periodically cycle. This way the power supplies (batteries) would be active for the same amount of time of a certain period.

In order to implement this system an “Embedded Matlab Function” had to be inserted into the simulink model. This block executes a script when activated. The activation is governed by the clock block. At the start of the simulation time a vector of thresholds is input to the units. The values of the vector correspond to the values seen in the previous paragraph. The

difference is that after a pre-determined period the vectors are rotated so that for example the threshold value of the first unit becomes the one of the second. Obviously this event happens simultaneously for all units.

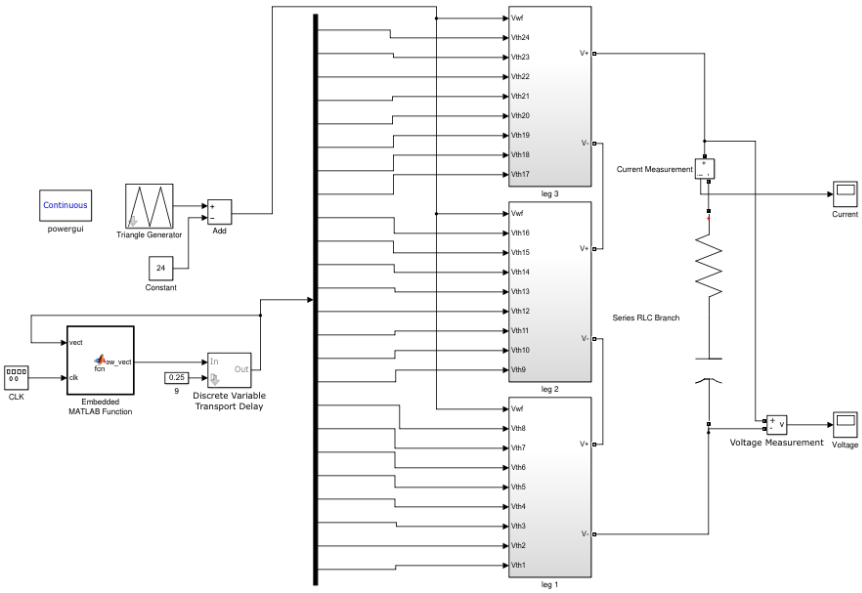

Figure 3.11 Cycling levels model

Fig. 3.12 shows the output voltage of each individual elementary unit. As it is evident after each period of the reference signal the threshold moves from a lower unit to a higher. After 24 periods a full cycle of the thresholds is completed and the algorithm is repeated. The numbering of the units is kept just for reference and is no more assigned to a particular threshold value.

This control method balances the discharges of the power supplies very efficiently especially for symmetric waveforms like the triangle. Sometimes though a more dynamic power balancing might be needed in order to react to power mismatch in a more immediate way rather than periodically. For this reason another balancing method has been developed.

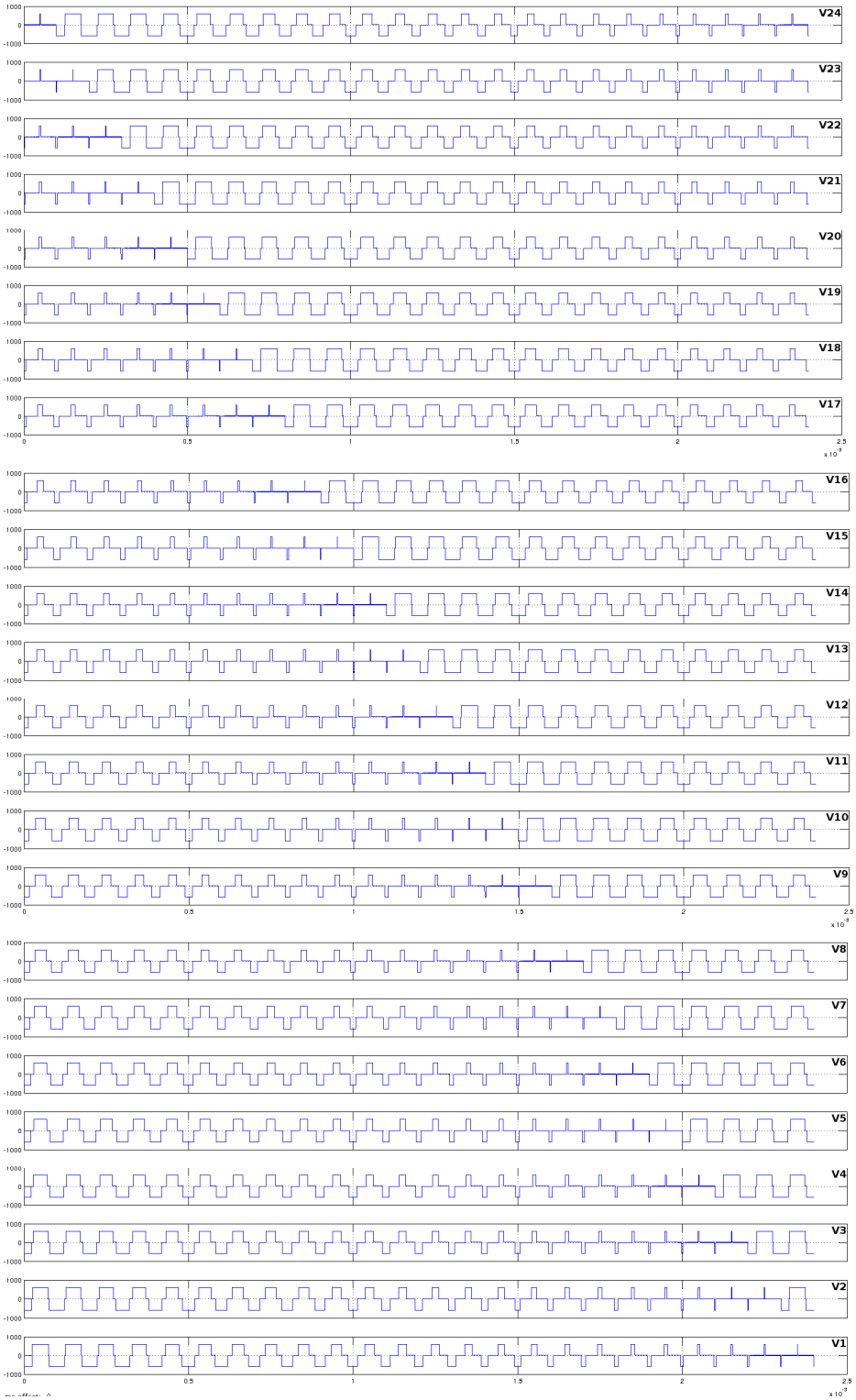

Figure 3.12 Cycling levels waveforms

3.6 Dynamic Balancing

A more complex balancing scheme has been implemented for cases where cycling the levels is not enough and a more immediate action is required. As seen the previous algorithm is a static method. In order to have a faster and more accurate algorithm a feedback loop had to be introduced. In particular the dynamic balancing method that is presented in this section requires a voltage and current measurement of each elementary level.

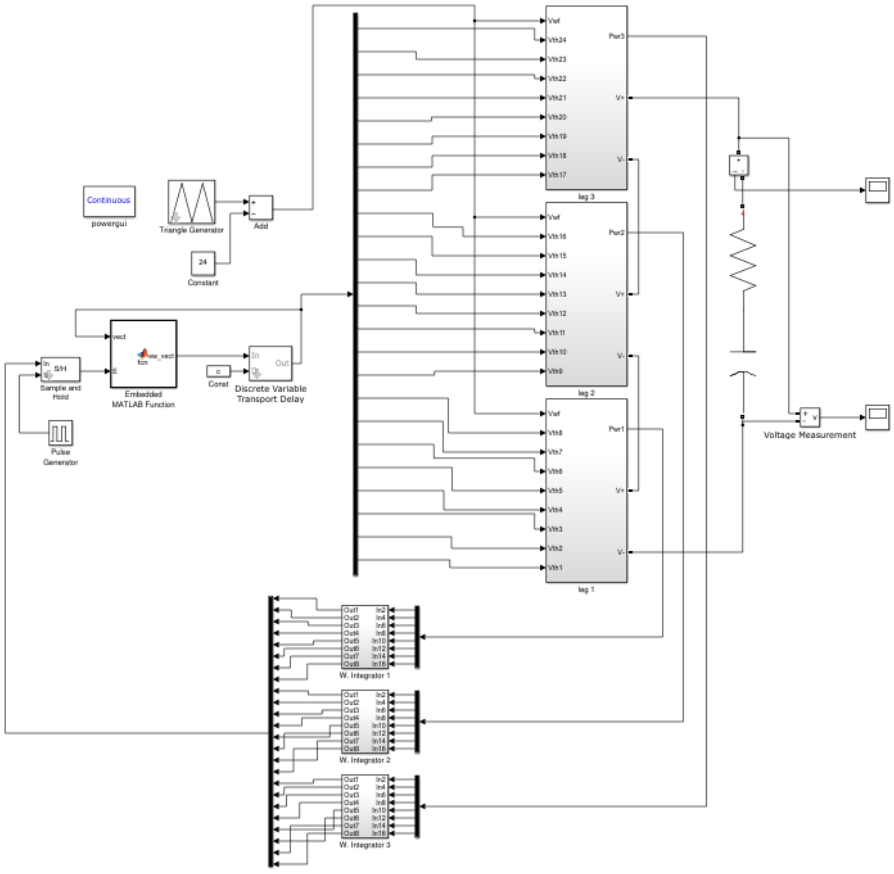

Figure 3.13 Dynamic balancing model

These measurements are multiplied and the instant power produced by each unit is calculated. In Fig. 3.13 the three

vectors Pwr1, Pwr2 and Pwr3 carry 8 element vectors that contain the calculated powers for each unit. These measurements are then fed into a windowed integrator

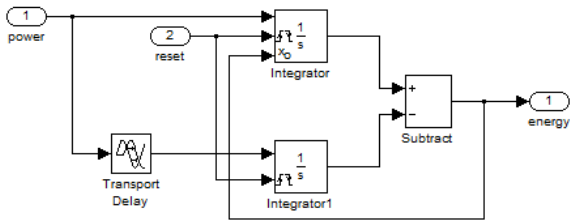

Figure 3.14 Windowed integrator

The integrator computes the integral value of the input power during a given period of time. This period is set to 50us which half of the period of the reference signal (10kHz). This calculation produces the provided energy by each unit.

The window integrator is composed of two integrator blocks the second one of which receives a delayed sample of the power. Thus by computing the difference between the two integrator blocks the energy in a given time frame is calculated.

A reset signal is necessary in order to avoid saturation. When this signal is triggered the output of the first integrator is set to the difference value between the two integrators while the second one is set to zero. This way the output of the windowed integrator is consistent.

A Sample and Hold block receives the 24 calculated energy values and samples them with a period of 50 us in order to provide constant values to the Embedded Matlab Function. In this case too, on the input of the block there is the *vect* vector with the old threshold values while on the output the new threshold values are generated though the *new_vect* every 50 us.

The implemented algorithm orders the new threshold values in function of the calculated energy values. The unit that has provided the most power during the previous sample period receives the highest threshold while the one that has provided the least energy receives the lowest threshold, thus it will be the one that will be active for the most time during the next cycle. What follows is the code executed when the Embedded Matlab Function is activated:

```
function new_vect = fcn(vect, energy)

new_vect=vect;

for i=0:1:(length(vect)-1)

      [max, posmax]=max(energy);
      new_vect(posmax)=23.5-i;
      energy(posmax)=0;

end;

end
```

A 24 iterations cycle is executed during which the maximum value of the energy vector is found as well as its position with the use of the *m(energy)* function. The highest threshold value is then assigned to the corresponding unit and the previously calculated maximum value of the energy is set to zero. This is done in order to find the second highest energy value then third etc.

Chapter 4

EXPERIMENTAL RESULTS

4.1 17 levels vs sinusoidal

The multilevel has been tested in the lab in a gradual way. The first experiments involved just few elementary units in order to be sure of the correct functioning of the multilevel. The first major step was when a stack of 8 units was put together.

Fig. 4.1 shows a triangular waveform. The peak to peak voltage is 9.6 kV and the frequency is 8 kHz. Note that in this experiment the zero step voltage was omitted. The plasma actuator has a length of 4 cm and the dielectric is 2 mm deep made of kapton.

The lower part of the figure shows the respective current measured on the low voltage electrode. As expected an impulsive type of current is seen. Peaks reach values of around 0.5 and can be detected only when there is a voltage step, either positive or negative.

Fig. 4.2 shows the voltage and current measured on the load when a sinusoidal power supply is applied. The peak to peak voltage as well as the frequency are the same like in the multilevel case.

A clear advantage of the multilevel current waveform is the lack of the capacitive component which generates that low frequency variation that can be seen on the sinusoidal power supply current graph. Plasma is only produced during discharges so having a low frequency component in the current

does not provide any effect. As a matter of fact it is a negative factor because it is a cause of inefficiency.

Another advantage of the multilevel inverter against the sinusoidal is the measured power delivered to the plasma actuator. The multilevel is able to provide 3.8 W vs the sinusoidal's 1.9 W.

These first results showed that the multilevel delivers more power to the plasma actuator and is generally more efficient.

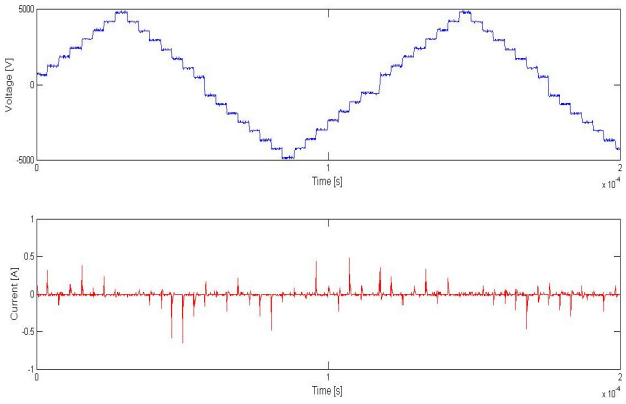

Figure 4.1 Triangular waveform

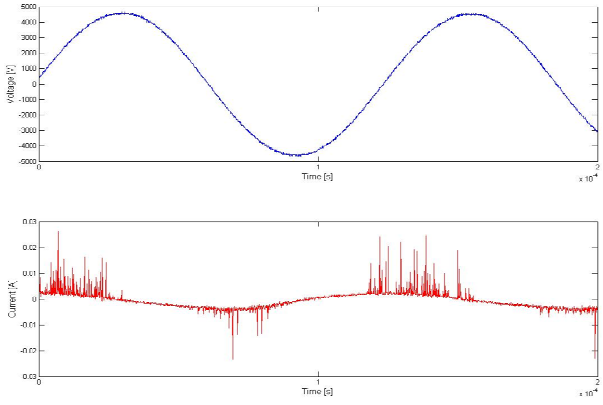

Figure 4.2 Sine waveform

4.2 Full voltage tests

This section illustrates a series of experimental results that have been done with different types of waveform. These tests were used to prove the functionality of the multilevel generator at its final configuration, generating 49 levels of output voltage. These tests were conducted in collaboration with Alenia Aermacchi both at the DEI labs as well as at the AAM labs.

The dielectric material that has been used was a Plexi 84. It is a special type of Polymethyl methacrylate. The use of this material is mandatory for avionic applications when a transparent thermoplastic surface has to be used because of the high robustness to corrosion and the long expected lifetime it can provide as opposed to other plastic materials. The thickness of the dielectric was 4 mm.

Both the high voltage and low voltage electrode were made of copper which comes in parts of tape that are stitched on the dielectric surface. The high voltage electrode was connected to the high voltage output connector of the multilevel while the low voltage electrode was connected to the low voltage output and to the ground.

The measurements were done using a Yokogawa Dl6054 digital oscilloscope. Voltage was measured with the use of a 20 kV voltage probe while the current sensing was done using a hall effect sensor probe. Due to the impulsive nature of the current its measurement has been particularly challenging to achieve. Other types of sensors were tested, like an amperometric transformer or even series connected resistor, but the Hall effect sensor probe was the one that gave the most reliable and realistic results.

The main purpose of the following tests was to compare the results with those given by a resonant converter. In particular the load matching of the resonant converter could happen only at a certain frequency of about 6.2 kHz. It was of particular interest to try to supply the plasma actuator at lower frequencies. That is why most of the results that will be shown were generated at lower frequencies with respect to the multilevel's maximum frequency of 20 kHz

4.2.1 Square waveform

Figure 4.3 shows the voltage and current measurements for a square waveform. The full 28.8 kV peak to peak voltage was applied to the actuator at 5 kHz frequency. The size of the electrodes was 40 cm in length and 1 cm in width

The shape of this type of waveform can be split into two regions. The first on is where all 24 H-bridges switch simultaneously and the voltage peak is generated. During a single period of the wave form this event happens twice, once from the lower negative point to the top positive point and once from the top positive point to the lower negative point.

The second region of the waveform is a long plateau were the voltage is kept a constant level. In this part of the waveform the state of all H-bridges is constant, no switching happens. In reality it can be seen that the plateau is not perfectly horizontal as there is a small slope both on the positive side as well as on the negative. This is due to high capacitive couplings that happen when the multilevel is functioning. This capacitive polarization generates a small overshoot of the voltage when more than one H-bridges are simultaneously switched to the

same direction. In this case, due to the fact that all H-bridges switch simultaneously this effect is very evident.

During this overshoot the voltage reaches a maximum value of about $\pm$15.7 kV. For the positive side of the voltage it can be seen that after this initial over-voltage there is a negative slope that leads to the actual 14.4 kV voltage of the multilevel. Vice versa for the negative voltage.

This phenomenon is not really a negative effect for the purpose of these experiments. As previously said plasma is formed when a discharge happens. Thus what is contributing to plasma generation are the current spikes that are generated. In fact the regions where the current is zero are have no real effect on the plasma. Therefore, a voltage overshoot that leads to a slightly higher current spike is actually a positive consequence. Obviously, that is not to say that this effect should not be controlled but in a restrained way and inside some margins it was intentionally accepted when testing the multilevel.

The measured current spike when peak-to-peak voltage switches happen is roughly 1.5 A both positive and negative. It should be noted that in the region when the voltage has a plateau the current is never actually zero. This happens because small discharges happen even when constant voltage is applied. This effect makes the calculation of the useful power provided to the plasma actuator quite difficult.

In order to get a rough estimate of the power delivered to load an average had to be calculated over a series of periods of the voltage and current measures. The square waveform’s power resulted in 67 W.

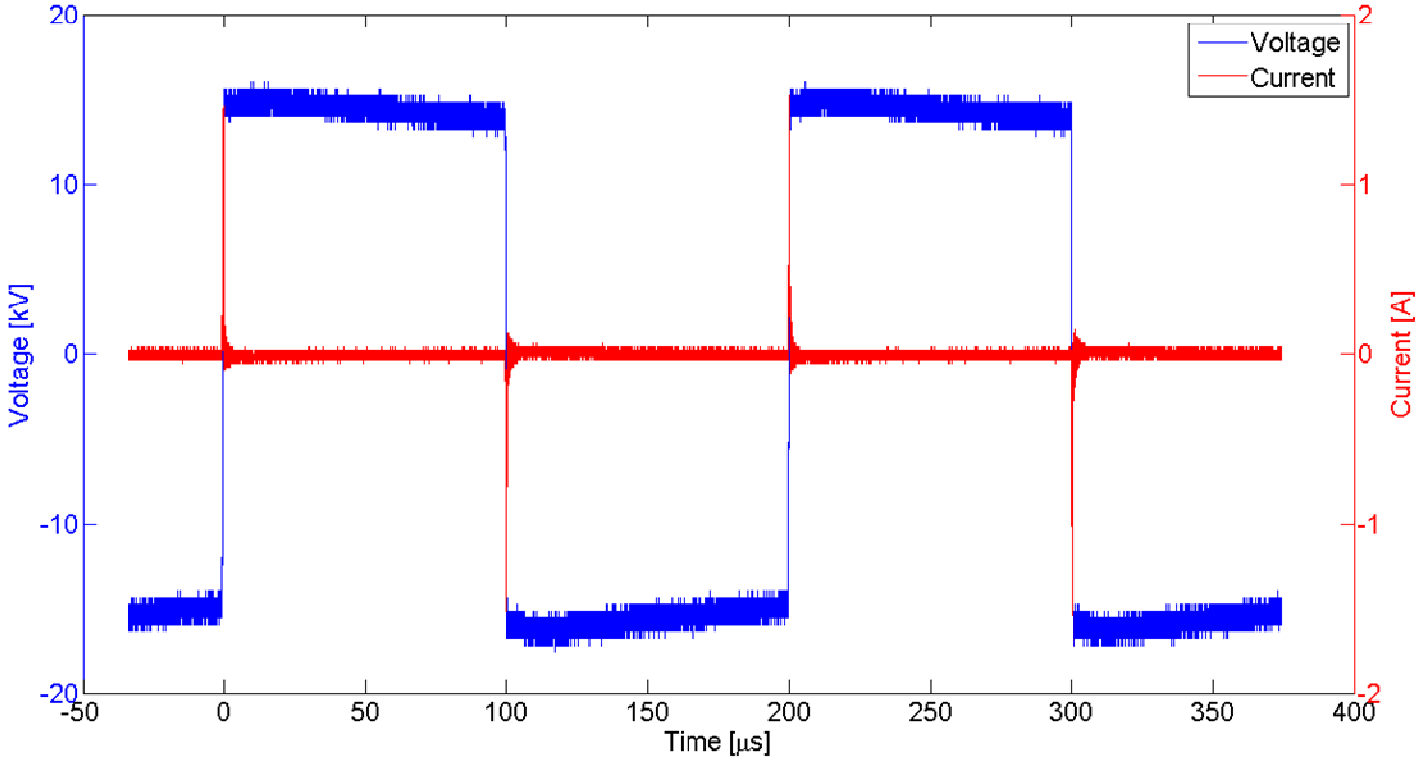

Figure 4.3 Square waveform

Figures 4.4 present a detailed view of both voltage and current waveforms during the negative and positive transients. In both cases the transient time for a peak-to-peak 28.8 kV switch is about 500 ns. This corresponds to a voltage rate of 60 kV/us. These measures prove the how well the multilevel performs in these situations. The voltage step is almost symmetric on both variations. As noted before a small ringing effect on the current is seen where it oscillates around the zero value.

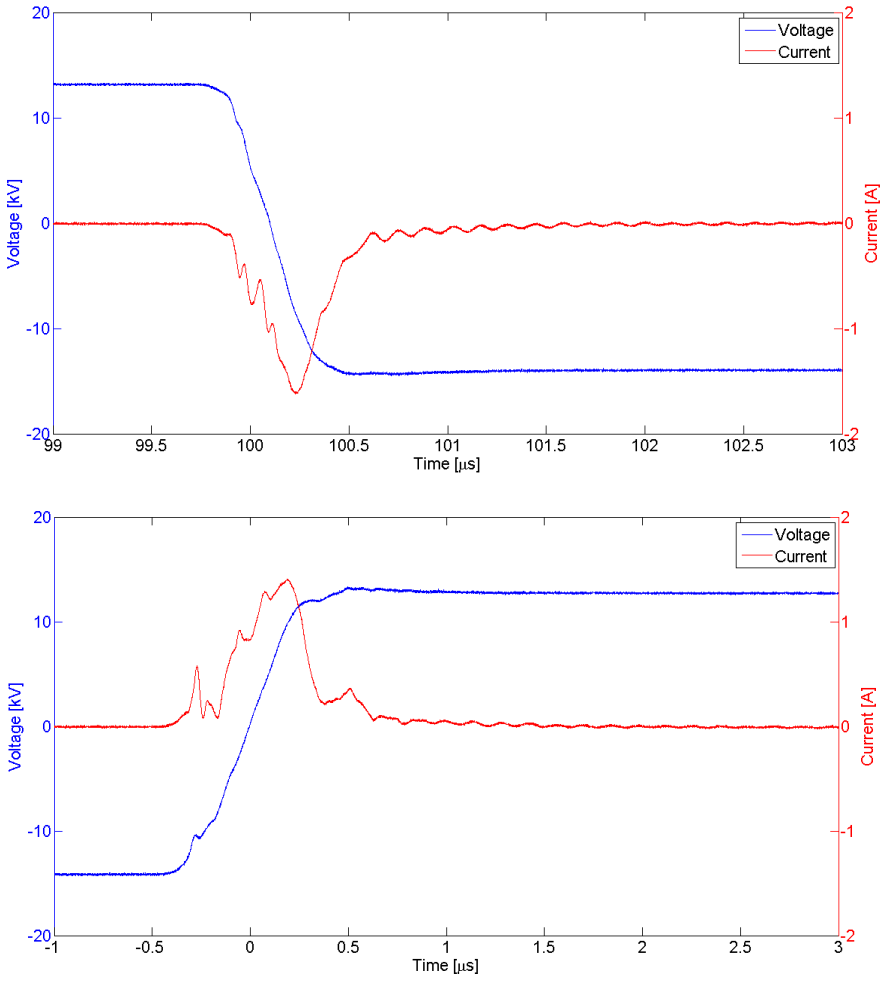

Figure 4.4 Detailed view of the voltage and the current

4.2.2 Triangular Waveform

Fig. 4.6 shows the voltage and current measurements for a triangular waveform at full voltage and at 4.9 kHz. The electrodes were 10 cm long. In this case the H-bridges have been switched two at a time, thus 12 positive steps and 12 negative steps can be counted. Each voltage step measures 1200 V. As it can be noted even though the peak voltage is the same as the square waveform the current peak is significantly lower due to the shorter electrodes and to the type of waveform. Maximum current is 0.15 A. In this case though the distribution of the spikes is also different. Due to the fact that the total voltage waveform is composed of many voltage steps the number of spikes during a single period is much bigger. In the end this results in more power delivered to the load as opposed to higher but scarce current spikes.

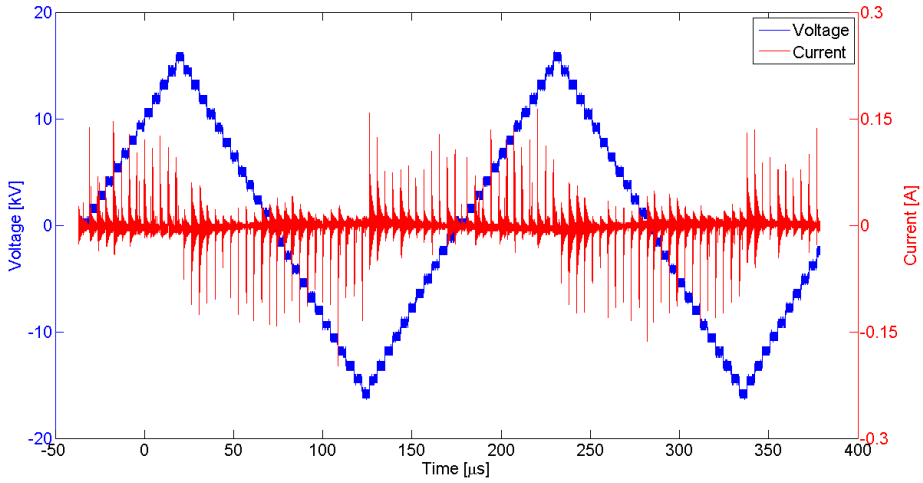

Figure 4.6 Triangular waveform

Fig. 4.7 shows the simulated version of the triangular waveform applied to a series R-C load. A plasma actuator can be quite difficult to model as it as the value of the impedance can dynamically change during the discharges. Therefore a

static load was chosen to be used in order to have a rough estimate of how the multilevel would behave.

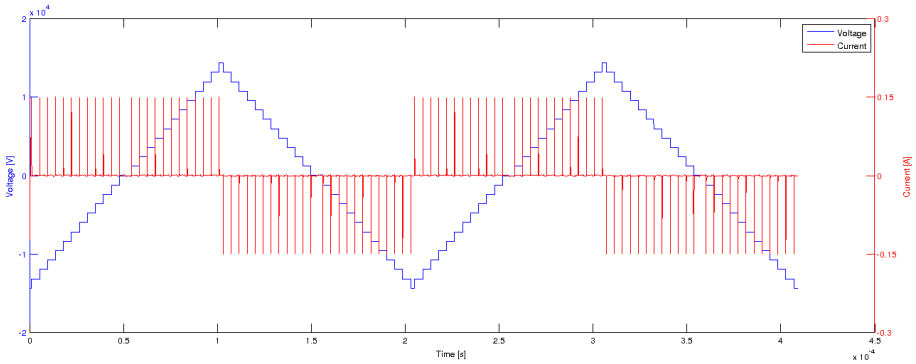

Figure 4.7 Simulated triangular waveform

The shape of the current is very close to the one that has been measured though the simulated one generates constant value spikes. This is not happening in the real system where the spikes have different values. This can be explained by the fact that as said the actual impedance of the actuator is dynamically varying during the experiments and also because capacitive couplings have not been taken into account in the simulation.

4.2.3 Sawtooth

Fig. 4.8 shows the measured voltage and current for a negative slope sawtooth waveform with 10 cm long electrodes. In this case all H-bridges have been used separately thus providing voltage steps of 600 V during the slope section. This type of waveform can be thought of as a mix between the triangular and the square waveform due to the fact that there is

a large current spike followed by lower though frequent spikes. The top current value has been measured to be 0.22.

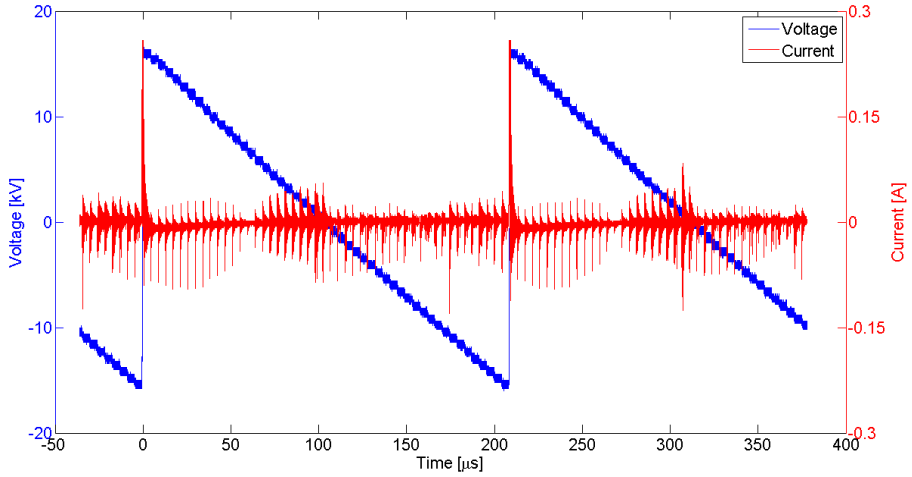

Figure 4.8 Sawtooth waveform

Fig. 4.9 Shows the simulated version of this waveform. The difference with the real one is more evident in this case. The current peaks where there is a high voltage switch though the rest of the spikes are much lower. As said the presented simulations are needed to get a rough estimate of the behaviour of the current not a perfect match.

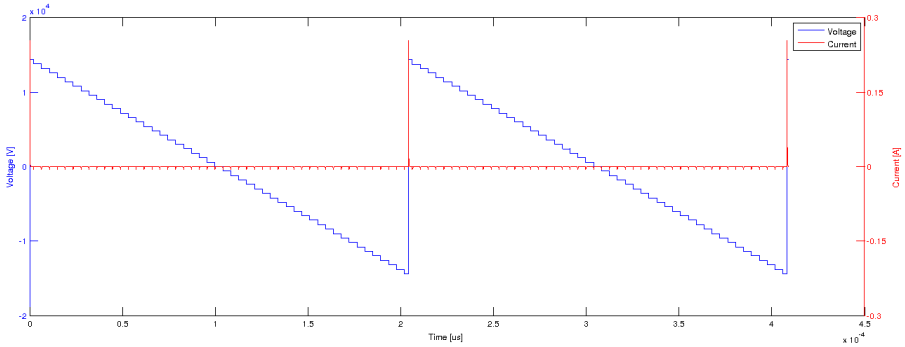

Figure 4.9 Simulated sawtooth waveform

4.2.4 Semi sinusoidal

Fig. 4.10 shows the flexibility of the multilevel in regard to the output waveform construction. Again electrodes were 10 cm long. Here a semi sinusoidal voltage waveform was generated. This type of output can be very interesting to test when comparing the results with a perfect sinusoidal waveform generated by a resonant converter. In this case, like for the triangular waveform more H-bridges switch simultaneously. This time though the number is not fixed and it depends on which part of the wave the switch happens.

In particular in order to form a sine waveform as close to a real one more H-bridges have to be switched when approaching the zero voltage level while on the top and lower parts of the waveform the H-bridges have to be singularly switched. For this reason the current spikes close to the zero region are bigger than the others, with the ones close to the higher and lower voltage levels being the lowest.

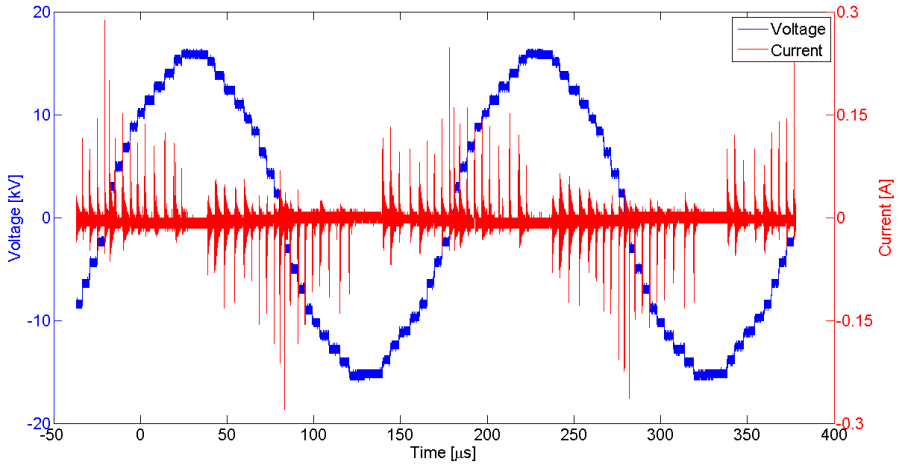

Figure 4.10 Semi sinusoidal waveform

In Fig. 4.11 a simulated sine voltage waveform is shown. Note that in this case a perfect sine wave is depicted. For this simulation the same comments as for what said for the triangular waveform simulation stand true.

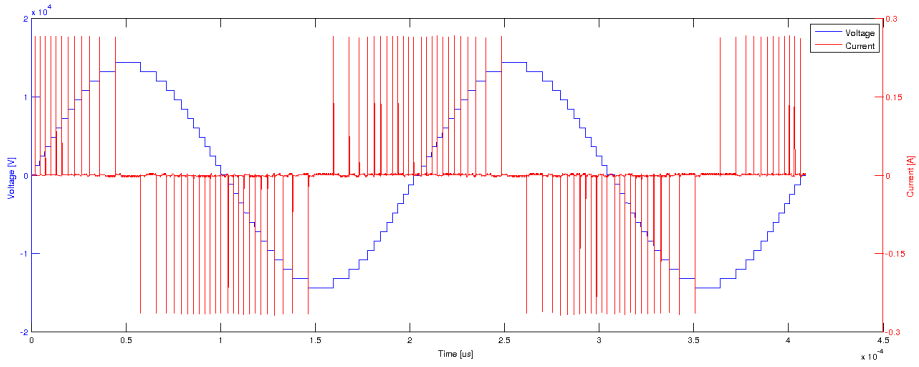

Figure 4.11 Sine waveform

4.2.5 Positive triangle

Fig. 4.12 is another display of how the multilevel within its resolution limits can generate arbitrary waveform. In particular an only positive triangular waveform at 10 kHz is shown. With 10 cm long electrodes the voltage peak value is still 14.4 kV while the H-bridges are switched 2 at the time. The measured current is significantly lower than the other cases and this type of waveform is not particularly efficient on a plasma actuator load.

Though, generating a voltage waveform with non zero average value can be a very interesting case study for how charged particles deposited on the borders of the dielectric react to an only positive alternating voltage. Obviously, the same type of waveform can be generated with negative voltage values too.

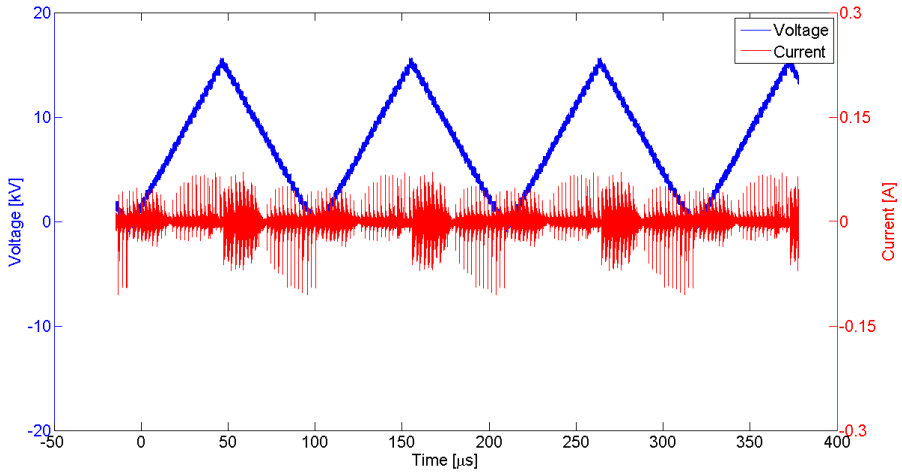

Figure 4.12 Positive triangular waveform

4.3 Velocity measures

This section provides some measured results with regard to the actual fluid dynamic force that has been generated with the plasma actuator when a multilevel AC voltage was applied. The measure of the fluid (air) speed has been done with the use of a Pitot tube sensor.

The used dielectric material was again a Plexi83 with a 4 cm thickness. The electrodes were 40 cm long and 1 cm wide. The measures have been done starting from two different distances from the end of the generated plasma and moving away from it. In particular 12 mm and 20 mm measures were executed. This was useful in order to better understand not only the intensity of the force but also the length. Different types of waveform were used.

Fig. 4.13 shows the measures starting at 12 mm. The reference here is the black curve which has been generated by a resonant converter. For each tested waveform 10 samples

were measured and then averaged in order to have a more stable result.

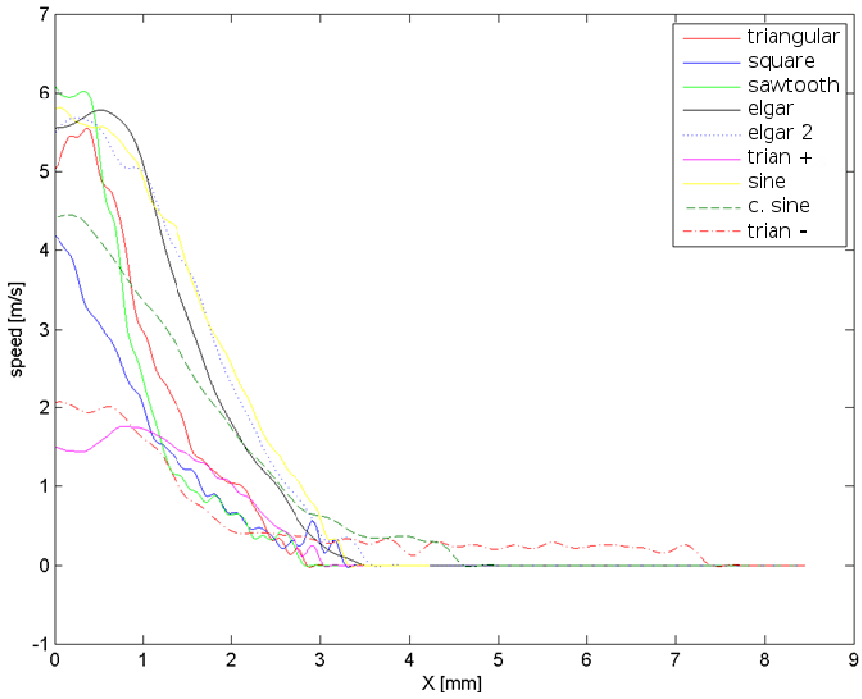

Figure 4.13 Velocity starting at 12 mm

As it can be seen most of the waveforms are outperformed by the resonant converter (black) with the semi sinusoidal (yellow) waveform almost matching this result. The absolute peak in fluid dynamic force though was measured with the sawtooth waveform (green) which has the absolute maximum value close to the plasma formation but then decreases very rapidly.

Fig. 4.14 shows the result with the pitot sensor starting at 20 mm. Apart from the positive and negative triangular waveforms (purple and dotted) that as already mentioned are not particularly efficient on plasma actuator loads

The remaining waveform provide closer results. The sawtooth is again the one that provides the top velocity.

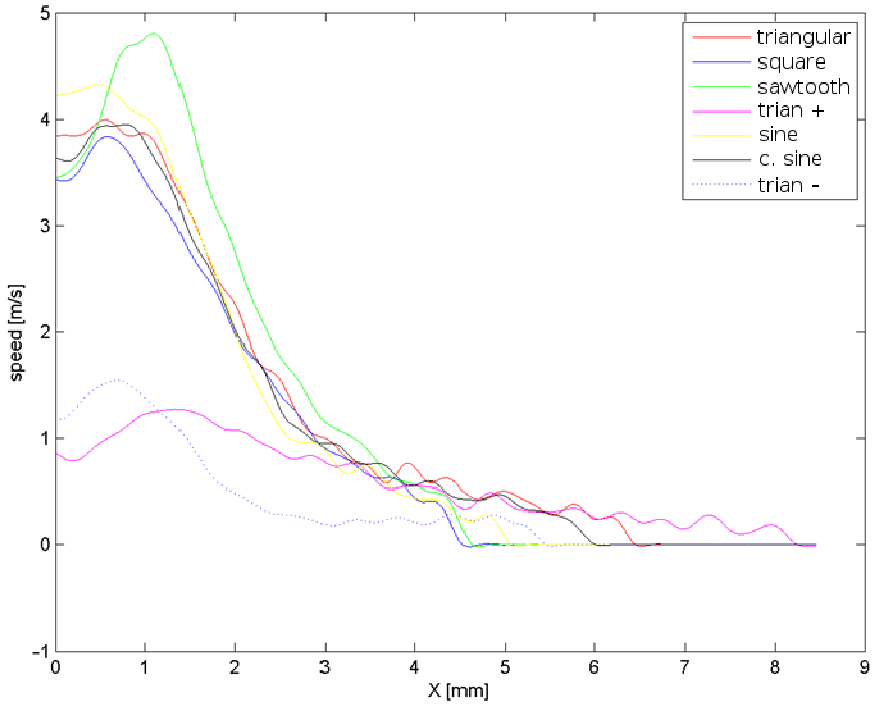

Figure 4.14 Velocity starting at 20 mm

Chapter 5

CONCLUSIONS

The realization of a high-voltage high-frequency arbitrary voltage generator has been the subject of this dissertation. All design steps have been shown as well as the final implementation. The experimental results show how the multilevel converter is able to actually generate high voltage high frequency arbitrary waveforms independently of the type of plasma actuator.

The presented system has been successfully accepted by Alenia Aermacchi as the reference model for the design of a multilevel converter which, as only difference, will be powered by AC voltage instead of batteries. As shown isolation issues can rise when using a transformer to power a cascaded inverter. Thus future investigations on this type of power supply are needed.

Another future development would be to fine tune the simulink model at IGBT level in order to have even more realistic results and not just a qualitative behaviour of the current. This would also permit to correctly model the load.

Finally, fluid dynamic effects of plasma actuators are still at primary research level. For this reason experimental results on velocity should by no means be considered completed. The implementation of the presented cascaded multilevel inverter opens up new possibilities for the study of the plasma actuators and provides an important tool for the continuation of this research.

[1] C. Tendero, C. Tixier, P. Tristant, J. Desmaison, P. Leprince, *"Atmospheric pressure plasmas: A review,"* Spectrochimica Acta Part B: Atomic Spectroscopy, vol. 61, No. 1, pp. 2-30, Jan. 2006.

[2] L. Bárdos, H. Baránková, *"Cold atmospheric plasma: Sources, processes, and applications,"* Thin Solid Films, vol. 518, No. 23, pp. 6705-6713, Sept. 2010.

[3] A. Fridman, A. Chirokov and A. Gutsol*. "Non-thermal atmospheric pressure discharges"* .J. Phys D: Appl Phys, 38: R1-R24, 2005.

[4] U. Kogelschatz. *"Atmospheric-pressure plasma technology"*. Plasma Phys. Control. Fusion, vol 46, issue 12B, B63-B75, 2004, DOI: 10.1088/0741-3335/46/12B/006.

[5] J.Y. Jeong, S. E. Babayan, V. J. Tu, J. Park, I. Henins, R. F. Hicks and G. S. Selwyn.. *"Etching materials with an atmospheric pressure plasmas jet"*. Plasma Sources Sci Technol, 7: 282-285, 1998.

[6] N. Yaman, E. Özdoğan, and N. Seventekin, *"Atmospheric plasma treatment of polypropylene fabric for improved dyeability with insoluble textile dyestuff"*, Fibers and Polymers, February 2011, Vol. 12, No. 1, pp. 35-41.

[7] S. Lerouge, M.R. Wertheimer and L'H. Yahia *"Plasma Sterilization: A Review of Parameters, Mechanisms, and Limitations"* Plasmas and Polymers, Vol. 6, No. 3, Sept. 2001.

[8] M. Been Chang, C. Chun-Cheng, *"Destruction and removal of toluene and MEK from gas streams with silent*

discharge plasmas " American Institute of Chemical Engineers. AIChE Journal; May 1997; 43, 5; pg. 1325

[9] G.J. Pietscha and V.I. Gibalovb *"Dielectric barrier discharges and ozone synthesis"* Pure&Appl. Chem.,Vol.70, No. 6, pp. 1169-1174,1998

[10] S. Min, G.A. Evrendilek, H.Q. Zhang, *"Pulsed Electric Fields: Processing System, Microbial and Enzyme Inhibition, and Shelf Life Extension of Foods,"* IEEE Trans. on Plasma Science, vol. 35, No. 1, pp. 59-73, Feb. 2007.

[11] A. H. El-Hag, S. H. Jayaram, M.W. Griffiths, *"Inactivation of Naturally Grown Microorganisms in Orange Juice Using Pulsed Electric Fields,"* Plasma Science, IEEE Transac¬tions on, vol. 34, iss. 4, pt. 2, pp. 1412-1415, Aug. 2006

[12] M. Laroussi*, "Low Temperature Plasma-Based Sterilization: Overview and State-of-the-Art,"* Plasma Processes and Polymers, vol. 2, iss. 5, pp. 391-400, Jun. 2005.

[13] G. Friedman, A. Gutsol, A.B. Shekhter, V.N. Vasilets, A. Fridman, *"Applied Plasma Medicine",* Plasma Processes and Polymers, Vol. 5, Issue 6, Article first published online: 16 Apr. 2008.

[14] T.C. Corke, C. Lon Enloe, S. P. Wilkinson, *"Dielectric Barrier Discharge Plasma Actuators for Flow Control,"* Annual Review of Fluid Mechanics, vol. 42, pp. 505-529, 2010.

[15] N. Benard, E. Moreau*, "Role of the electric waveform supplying a dielectric barrier discharge plasma actuator,"* Applied Physics Letters, vol. 100, iss. 9, ref. 193503, May 2012.

[16] A. Cristofolini, C.A. Borghi, and G. Neretti *"Charge distribution on the surface of a dielectric barrier*

discharge actuator for the fluid-dynamic control", J. of Appl. Phys. 113, 143307 (2013), DOI: 10.1063/1.4799159.

[17] A. Cristofolini, G. Neretti, and C. A. Borghi, *"Effect of the charge surface distribution on the flow field induced by a dielectric barrier discharge actuator"* J. Appl. Phys. 114, 073303 (2013); doi: 10.1063/1.4817378.

[18] Song Guo, *"An Investigation of Dielectric Barrier Discharge Based Plasma Actuator Designs With Enhanced Performance In Active Flow Control,"* PhD dissertation, University of Minnesota

[19] J. Rodriguez, S. Bernet, Bin Wu, J. O. Pontt, *"Multilevel Voltage-Source-Converter Topologies for Industrial Medium-Voltage Drives,"* IEEE Trans. on Industrial Electronics, vol. 54, iss. 6, pp. 2930-2945, Dec. 2007

[20] J. Rodriguez, Jih-Sheng Lai, Fang Zheng Peng, *"Multilevel inverters: a survey of topologies, controls, and applications,"* IEEE Trans. on Industrial Electronics, vol. 49, iss. 4, pp. 724-738, Aug 2002

[21] Mitsubishi Electric, *"Dual-In-Line Package Intelligent Power Module,"* PS22A74 datasheet, Jan. 2012.